Cell

General Protein Diffusion Barriers Create Compartments within Bacterial Cells

Susan Schlimpert,[1,3,10] Eric A. Klein,[5,10] Ariane Briegel,[7] Velocity Hughes,[8] Jörg Kahnt,[2] Kathrin Bolte,[4] Uwe G. Maier,[4,9] Yves V. Brun,[8] Grant J. Jensen,[6,7] Zemer Gitai,[5] and Martin Thanbichler[1,3,9,*]
[1]Max Planck Research Group "Prokaryotic Cell Biology"
[2]Department of Ecophysiology
Max Planck Institute for Terrestrial Microbiology, Karl-von-Frisch-Straße 10, 35043 Marburg, Germany
[3]Laboratory for Microbiology
[4]Laboratory for Cell Biology
Department of Biology, Philipps-Universität, Karl-von-Frisch-Straße 8, 35043 Marburg, Germany
[5]Department of Molecular Biology, Princeton University, Princeton, NJ 08544, USA
[6]Howard Hughes Medical Institute
[7]Division of Biology
California Institute of Technology, 1200 East California Boulevard, Pasadena, CA 91125, USA
[8]Department of Biology, Indiana University, 1001 East 3rd Street, Bloomington, IN 47405, USA
[9]LOEWE Center for Synthetic Microbiology, Hans-Meerwein-Straße, 35043 Marburg, Germany
[10]These authors contributed equally to this work
*Correspondence: thanbichler@mpi-marburg.mpg.de
http://dx.doi.org/10.1016/j.cell.2012.10.046

SUMMARY

In eukaryotes, the differentiation of cellular extensions such as cilia or neuronal axons depends on the partitioning of proteins to distinct plasma membrane domains by specialized diffusion barriers. However, examples of this compartmentalization strategy are still missing for prokaryotes, although complex cellular architectures are also widespread among this group of organisms. This study reveals the existence of a protein-mediated membrane diffusion barrier in the stalked bacterium *Caulobacter crescentus*. We show that the *Caulobacter* cell envelope is compartmentalized by macromolecular complexes that prevent the exchange of both membrane and soluble proteins between the polar stalk extension and the cell body. The barrier structures span the cross-sectional area of the stalk and comprise at least four proteins that assemble in a cell-cycle-dependent manner. Their presence is critical for cellular fitness because they minimize the effective cell volume, allowing faster adaptation to environmental changes that require de novo synthesis of envelope proteins.

INTRODUCTION

Proper spatiotemporal regulation of protein localization and mobility is crucial for cellular organization and development. In eukaryotes, proteins are commonly sorted to subcellular compartments such as the endoplasmatic reticulum or the Golgi apparatus, where they are separated from other cellular regions by a membrane bilayer. In addition, membrane systems can themselves be compartmentalized into functionally distinct domains by protein-mediated diffusion barriers, a compartmentalization strategy that is critically involved in the differentiation of cellular extensions such as buds, axons, dendritic spines, or primary cilia (Caudron and Barral, 2009). In most cases, the precise composition of the diffusion barriers and their mechanisms of function are still unclear. Similar to eukaryotes, prokaryotic cells have evolved strategies to compartmentalize proteins within the cell. These include the formation of various kinds of intracytoplasmic membrane vesicles or so-called microcompartments, highly specialized reaction chambers that encapsulate a defined set of metabolic enzymes in a protein shell (Murat et al., 2010). However, protein-mediated diffusion barriers with a role in membrane organization have not been identified in prokaryotes so far, although cellular extensions are also widespread among this group of organisms.

The Gram-negative bacterium *Caulobacter crescentus* (henceforth *Caulobacter*) develops a polar stalk that is formed by local extension of the cell body. It largely consists of cell envelope (i.e., outer membrane, peptidoglycan, and inner membrane) surrounding a thin cytoplasmic core devoid of DNA, ribosomes, and most cytoplasmic proteins (Ireland et al., 2002; Poindexter and Cohen-Bazire, 1964; Wagner et al., 2006). At its tip, the stalk carries an adhesive organelle (holdfast) mediating permanent surface attachment (Curtis and Brun, 2010). Moreover, it is segmented at irregular intervals by so-called cross-bands (Poindexter and Cohen-Bazire, 1964), disk-like structures that traverse the entire width of the stalk perpendicular to the long axis of the cell. Cross-bands are observed in a variety of prosthecate species and were hypothesized to have an architectural or stabilizing function (Jones and Schmidt, 1973; Poindexter and Cohen-Bazire, 1964; Schmidt, 1973; Schmidt and Swafford, 1975). However, their precise role and molecular composition

have remained unclear because the lack of mutants has so far prevented the elucidation of cross-band biogenesis and function.

Previous studies have established that cross-band formation is coupled to cell-cycle progression (Poindexter and Staley, 1996). Early in the *Caulobacter* life cycle, the polar flagellum is substituted for a stalk, marking the developmental reprogramming of a motile, DNA replication-arrested swarmer cell into a sessile, replication-competent stalked cell. After transition into S phase, the stalked cell elongates, assembles a new flagellum at the pole opposite the stalk, and finally divides asymmetrically to produce a new swarmer cell and a stalked cell. During the late stages of cell division, a new cross-band is added at the stalk base (Poindexter and Staley, 1996). It is then gradually displaced as the stalk elongates by insertion of new cell wall material at the junction between the stalk and the cell body (Schmidt and Stanier, 1966; Seitz and Brun, 1998; Smit and Agabian, 1982). Notably, stalk extension is significantly stimulated in response to phosphate starvation (Gonin et al., 2000). Based on this observation, current models suggest that the stalk promotes phosphate uptake by increasing the surface area of the cell. Because the ABC transporter complex that translocates phosphate across the inner membrane (PstCAB) is restricted to the cell body, phosphate was proposed to be shuttled from the stalk to the cell body by the periplasmic phosphate-binding protein PstS (Wagner et al., 2006).

Here, we demonstrate that cross-bands represent multiprotein complexes that act as diffusion barriers separating the *Caulobacter* stalk and cell body into functionally independent domains. Whereas eukaryotic diffusion barriers are mainly involved in organizing lipids or membrane proteins, cross-bands restrict the diffusion of both membrane-associated and soluble proteins. They provide cells with a significant fitness advantage by retaining newly synthesized membrane and periplasmic proteins in the cell body. This compartmentalization strategy minimizes the physiologically active part of the cell envelope, reducing the energy cost for protein synthesis and allowing faster adaptation of the cell envelope proteome to changing environmental conditions.

RESULTS

The *Caulobacter* Cell Is Compartmentalized by Protein Diffusion Barriers

When grown in phosphate-limiting conditions, *Caulobacter* cells display highly elongated stalks (Gonin et al., 2000). The resulting increase in the cellular surface area-to-volume ratio was proposed to facilitate phosphate scavenging, mediated through the shuttling of phosphate from the stalk to the cell body by the periplasmic phosphate-binding protein PstS (Wagner et al., 2006). To assay PstS mobility, we performed both FLIP (fluorescence loss in photobleaching) and FRAP (fluorescence recovery after photobleaching) studies of cells expressing a functional PstS-mCherry fluorescent protein fusion (Figures S1A and S1B available online). When a laser pulse was applied to the stalk-distal cell pole, fluorescence was lost throughout the cell body but not within the stalk (Figure 1A). Control experiments with fixed cells verified that the FLIP/FRAP setup used can bleach a small subregion of the cell and that protein diffusion is required for the total loss of fluorescence observed (Figures S1C and S1D). Thus, PstS-mCherry molecules can readily diffuse within the cell body periplasm but not across the stalk-cell body boundary, challenging the model of PstS-mediated phosphate shuttling. To test whether the observed diffusion barrier was bidirectional, we photobleached PstS-mCherry molecules in the stalk and, consistently, detected no recovery of stalk fluorescence (Figure 1B). Furthermore, when a laser pulse was applied to the tip of the stalk, PstS-mCherry fluorescence decreased only in a region close to the tip (Figure 1C), suggesting the existence of additional intrastalk compartmentalization.

Identification of Novel Stalk Proteins that Localize in a Cross-Band-like Pattern

Assuming a potential link between formation of the diffusion barrier and stalk biogenesis, we sought to identify the constituents of the barrier structure by focusing on uncharacterized open reading frames that were transcriptionally upregulated at the onset of stalk formation (McGrath et al., 2007). Candidate genes were fused to *mcherry* and ectopically expressed from a xylose-inducible promoter (P_{xyl}). Microscopic analysis of the resulting fluorescent protein fusions turned our attention to two conserved hypothetical proteins, CCNA_02562 and CCNA_02561 (Marks et al., 2010), that produced distinct foci distributed at irregular intervals along the length of the stalk. The two proteins, which are encoded in a putative operon, were designated StpA and StpB (*St*alk *p*rotein *A* and *B*), respectively (Figure 2A).

Prompted by the similar localization patterns of StpA and StpB, we tested whether the two proteins could interact with each other. Coimmunoprecipitation analysis followed by immunodetection showed that StpA indeed cosedimented with hexahistidine-tagged StpB (Stp-His) (Figure 2B), indicating that the two proteins formed a complex. Further analysis of the immunoprecipitates by mass spectrometry led to the identification of two additional stalk proteins, StpC (CCNA_02560) and StpD (CCNA_02271). Interestingly, *stpC* is likely to be cotranscribed with *stpA* and *stpB*, supporting the idea that the three gene products are functionally related. Fluorescently tagged StpC and StpD displayed the characteristic multifocus localization pattern observed for StpA and StpB and colocalized with StpA and StpB in the stalk (Figure 2C). Collectively, these biochemical interaction and colocalization data suggest that the four Stp proteins assemble into a multisubunit complex. Of note, the bodies of cells producing fluorescently tagged Stp proteins displayed higher fluorescence when grown in low-phosphate medium. This effect was not due to instability of the fluorescent protein fusions (Figures S2A and S2B) but may result from starvation-induced changes in gene expression and growth dynamics.

Bioinformatic analysis showed that StpB, StpC, and StpD lack known functional domains. StpA, by contrast, harbors three Sel1-like motifs, proposed to mediate protein-protein interactions (Blatch and Lässle, 1999). In addition, StpA, StpC, and StpD are each predicted to possess a single transmembrane helix close to the N terminus, whereas StpB is predicted to be a soluble periplasmic protein (Figure 2D). Protein fractionation experiments confirmed that StpA, StpC, and StpD exclusively

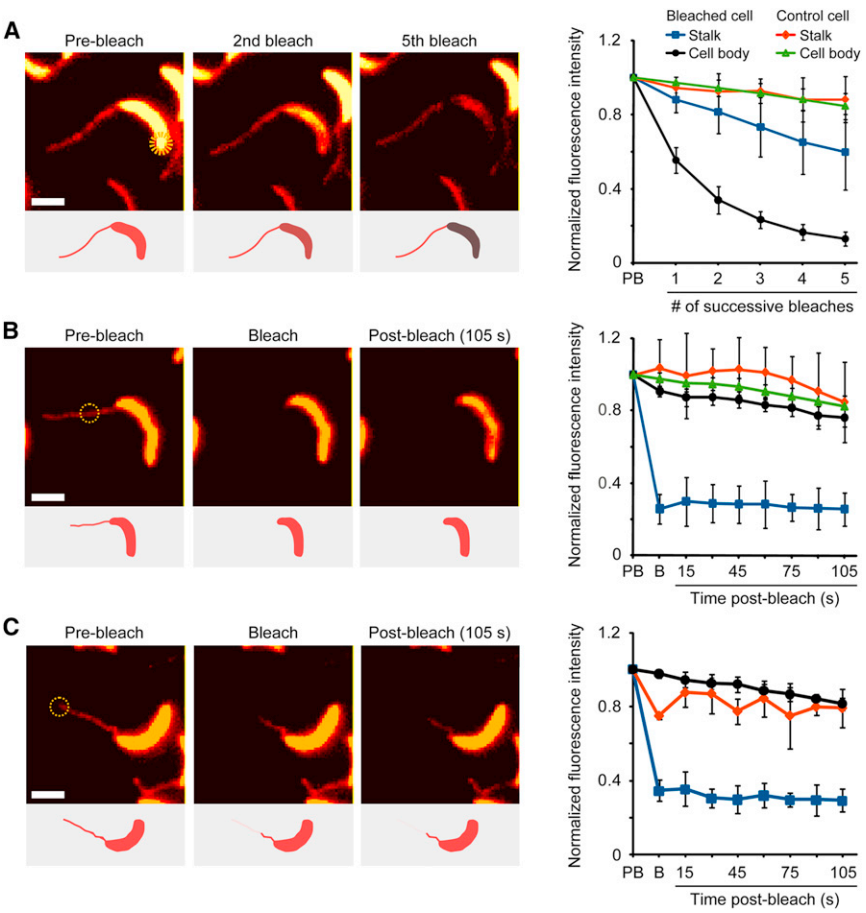

Figure 1. A Diffusion Barrier Compartmentalizes the *Caulobacter* Periplasm

(A–C) Diffusion of a xylose-inducible PstS-mCherry fusion assayed with FLIP (A) and FRAP (B and C). Cells (EK363) were bleached with seven ~4 nsec pulses in the region indicated by yellow circles. Bleaching was performed either multiple times in succession (A) or once followed by a 105 s recovery (B and C). Insets show schematic representations of the results, and graphs show the quantification of fluorescence in multiple cells (A: $n = 6$, $p < 0.0002$; B: $n = 7$, $p < 2 \times 10^{-7}$; C: $n = 3$, $p < 0.002$; p values: stalk versus cell body at the final timepoint; error bars = SD). Fluorescence intensities were measured in the stalk (blue) and cell body (black) of the bleached cell or in the stalk (red) and cell body (green) of a nearby control cell. For intrastalk bleaching, the bleached (blue) and unbleached (red) portions of the stalk as well as the cell body (black) fluorescence were quantified. The color-maps of the fluorescent images were scaled for easier visualization. However, all quantifications were performed with raw image data. The fluorescence intensity of each region of interest was normalized to its prebleach intensity. Abbreviations: PB, prebleach; B, bleach. Scale bars, 2 μm. See also Figure S1.

cosedimented with the cell membranes, whereas StpB was detected in both the membrane and the soluble protein fractions (Figure 2E). Notably, StpB was completely soluble in StpA-deficient cells, suggesting that StpA functions to tether StpB to the inner membrane. To further clarify the subcellular localization and membrane topology, we engineered C-terminal fusions of StpA, StpB, StpC, and StpD to a TEM-1 β-lactamase reporter, which needs to be translocated to the periplasm in order to confer resistance to β-lactam antibiotics. Expression of each of the four fusion proteins restored resistance to a β-lactam-sensitive reporter strain, demonstrating that StpB and the C-terminal portions of StpA, StpC, and StpD are positioned in the periplasmic space (Figure 2F).

The StpABCD Complex Forms Static Cross-band Structures

The Stp proteins show the same localization pattern as cross-bands and are, at least in part, conserved in other stalked bacteria that synthesize cross-bands, such as *Brevundimonas* and *Asticcacaulis* species (Figure S2D). To investigate whether they play a role in cross-band formation, we examined stalk ultrastructure in a Δ*stpAB* mutant by electron cryotomography (ECT). In tomograms of wild-type cells, cross-bands appeared as distinct densities that transect the inner membrane, peptidoglycan and outer membrane layers as well as the cytoplasmic core of the stalk (Figure 3A and Movie S1). Intriguingly, in StpAB-deficient cells, cross-bands were undetectable, whereas stalk length and morphology remained unperturbed, indicating that cross-band formation is not required for stalk biogenesis per se (Figure 3A). Strains lacking *stpC* or *stpD*, by contrast, still exhibited clearly discernible cross-bands (Figure S3A).

Next, we compared the frequency of StpB-mCherry foci and cross-bands in phosphate-starved wild-type cells as visualized by fluorescence and transmission electron microscopy, respectively (Figures 3B and 3C). The data revealed that Stp complexes showed the same average spacing (2.5 to 3 μm) as cross-bands. To determine whether the Stp complex colocalized with cross-bands, we analyzed phosphate-starved cells producing StpB-mCherry ($n = 11$) by correlated light microscopy and ECT. Alignment of ECT slices with fluorescence micrographs of the same region verified that the StpABCD complex invariantly assembles at the sites of cross-band formation (Figures 3D and S3B).

The Stp proteins lack domains with enzymatic activity and may therefore have a structural role. Indeed, when StpB-mCherry foci were photobleached, the fluorescence signal did not recover over time, and the intensity of neighboring StpB-mCherry foci remained unchanged (Figure 3E). Identical results were obtained for fluorescently tagged StpA, StpC, and StpD (data not shown). The four Stp proteins thus assemble into static multiprotein scaffolds that localize to the same subcellular sites as cross-bands. Previously, cross-bands were proposed to consist of peptidoglycan (Schmidt, 1973), with their synthesis depending on the essential cell division protein FtsZ (Divakaruni

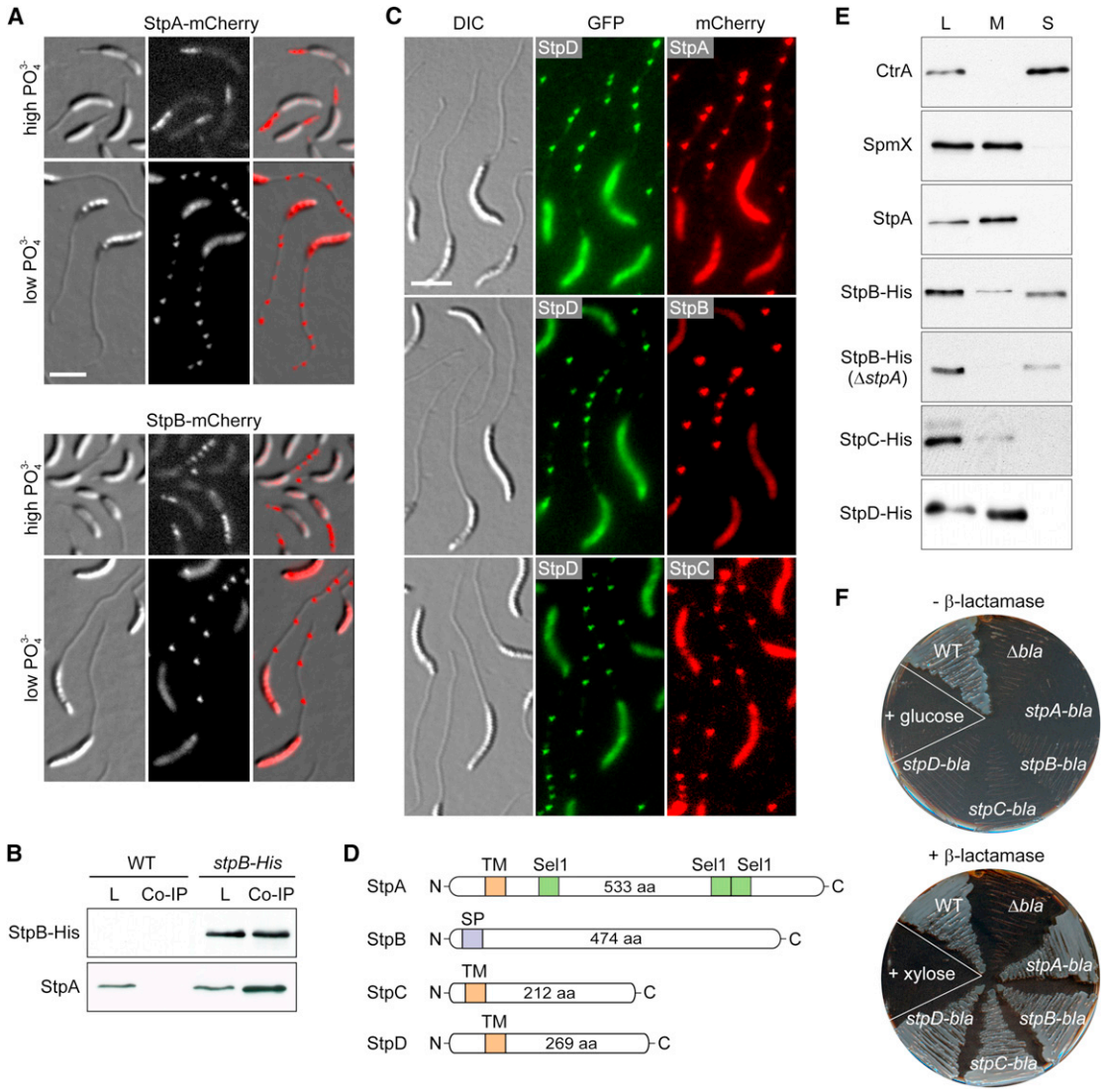

Figure 2. Identification and Subcellular Localization of Novel Stalk Proteins

(A) Stalk localization of StpA-mCherry (SW33) and StpB-mCherry (SW30) produced from the xylose-inducible P_{xyl} promoter after 24 hr of growth in phosphate-rich (M2G, high PO_4^{3-}) or phosphate-poor medium (M2G^{-P}, low PO_4^{3-}) containing 0.3% xylose.

(B) Coimmunoprecipitation analysis of *stpB*-His (SS233) and wild-type cells reveals an interaction between StpA and StpB. Whole-cell lysates (L) and eluates from coimmunoprecipitation experiments (Co-IP) were subjected to immunoblot analysis with anti-His and anti-StpA antibodies.

(C) StpA,B,C,D localization in stalks is reminiscent of the distribution of cross-bands. Cells of strain SS243 (*stpD;;stpD-gfp* P_{xyl}::P_{xyl}-*stpA-mcherry*), SS388 (*stpB;;stpB-mcherry stpD;;stpD-gfp*), and SS389 (*stpC::stpC-mcherry stpD;;stpD-gfp*) were grown in M2G^{-P} for 24 hr. Synthesis of StpA-mCherrry was induced with 0.3% xylose for 24 hr.

(D) Schematic depicting the domain organization of the Stp proteins with the predicted transmembrane domains (orange), the signal peptide (purple), and the Sel1 motifs (green).

(E) Cell fractionation analysis reveals that StpA, StpC, and StpD are membrane-bound proteins, whereas StpB is soluble. Whole-cell lysates (L) and the corresponding membrane (M) and soluble (S) fractions of cells producing His-tagged Stp proteins (SS233, SS220, SS244, and SS247) were subjected to western blot analysis with an anti-StpA or anti-His antibody. Fractionation efficiency was verified by probing the same fractions with anti-CtrA and anti-SpmX antibodies. Note, the absence of *stpA* and *stpAB* does not reduce the cellular levels of StpB and StpC, respectively (Figure S2C).

(F) The Stp proteins are targeted to the periplasm. The TEM-1 β-lactamase gene (*bla*) was fused to the 3′ end of *stpA*, *stpB, stpC*, and *stpD*, respectively. The gene fusions were placed under the P_{xyl} promoter in a β-lactam-sensitive reporter strain. Cells (SS165, SS172, SS273, SS274) were patched on PYE agar containing ampicillin and either 0.2% glucose or 0.3% xylose. Scale bars, 3 μm. See also Figure S2.

et al., 2007). However, we found that stalks of a conditional *ftsZ* mutant still displayed cross-bands (Figure S4A) and continued to accumulate StpB-mCherry foci with the typical cross-band-like distribution pattern (Figure S4B), supporting the idea that cross-bands represent macromolecular assemblies of StpABCD rather than cell wall material.

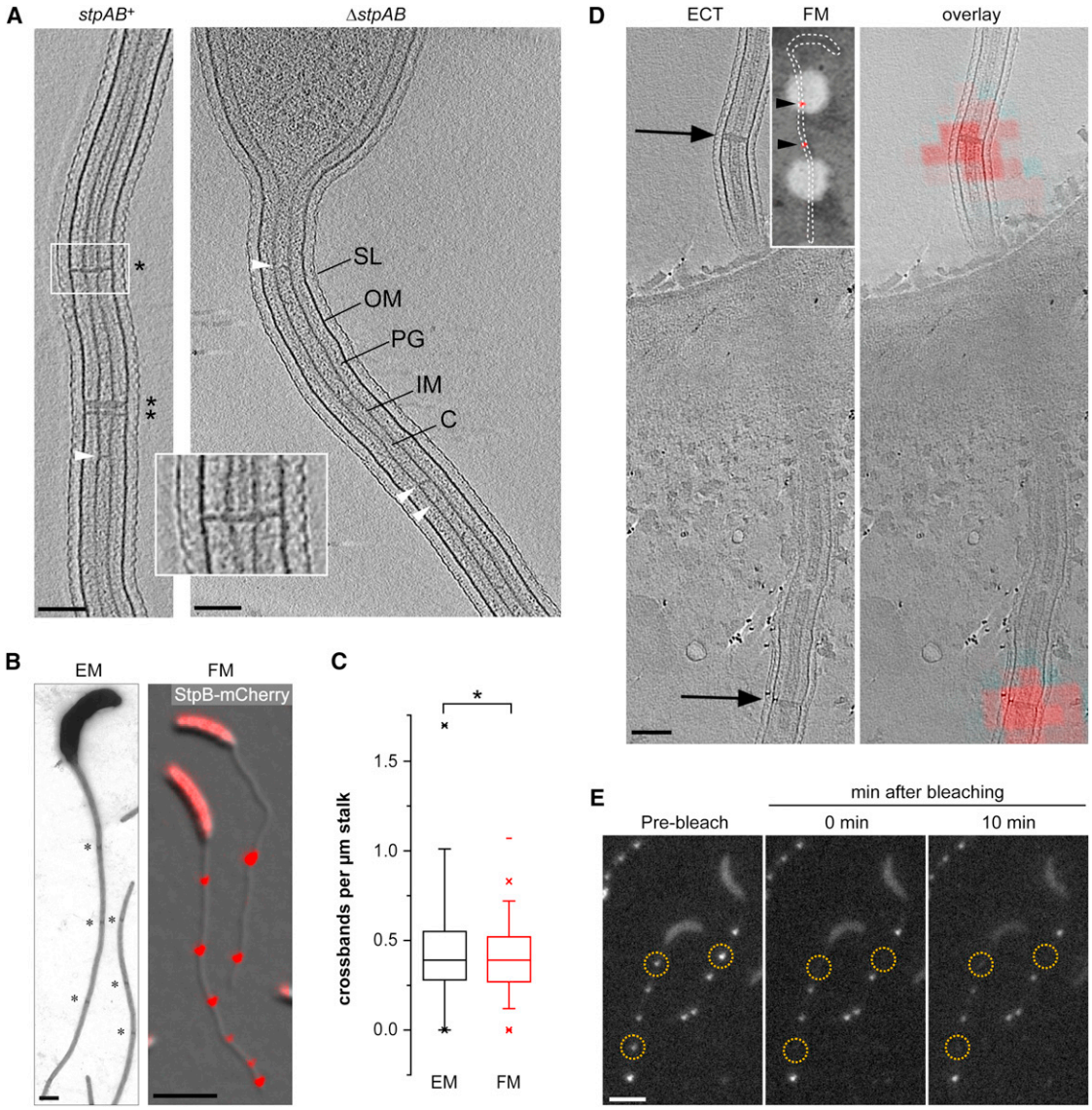

Figure 3. Cross-Bands Are Static Multiprotein Complexes

(A) StpAB-deficient cells consistently lack cross-bands. Cells with and without *stpAB* (SW51, n = 8) were grown in PYE and imaged by ECT. The images show a longitudinal section of the stalk. Asterisks denote cross-bands. Arrowheads point at unidentified structures spanning the stalk core. Scale bars, 100 nm.

(B and C) The distribution of StpB-mCherry foci reflects the distribution of cross-bands in stalks. Cells of strains CB15N (WT) and SS160 (*stpB-mcherry*) were grown in M2G^{-P} and imaged by transmission electron (EM) or fluorescence (FM) microscopy, respectively. From the respective images, the number of cross-bands (n = 68 cells) and StpB-mCherry foci per μm stalk (n = 316 cells) was quantified (*p > 0.2, t test). Asterisks denote cross-bands. Scale bars, 500 nm (EM) and 3 μm (FM). Box plots show the median and interquartile range (box), the 5th and 95th percentile (whiskers), the sample minimum and maximum (–), and outliers (x).

(D) StpB spatially overlaps with cross-bands. Strain SW30 (P_{xyl}::P_{xyl}-*stpB-mcherry*) was grown in M2G^{-P} with 0.3% xylose. Cells were fixed on EM grids and imaged first by low-magnification phase contrast/fluorescence microscopy (inset; arrowheads indicate StpB-mCherry foci) and then by ECT. Shown is an ECT slice of a stalk with arrows pointing to cross-band structures (left) and the respective correlated image showing the ECT slice overlayed with a fluorescence micrograph of the same region (right). Scale bar, 100 nm.

(E) FRAP analysis reveals that cross-bands are static protein complexes. Cells of strain SS160 (*stpB-mcherry*) were cultured in M2G^{-P} and imaged by fluorescence microscopy to identify StpB-mCherry localization. A laser pulse was applied to selected regions (yellow circles), and StpB-mCherry signals were bleached. Cells were imaged immediately and 10 min after the laser pulse. Scale bar, 3 μm. See also Figure S3.

StpA Is the Central Regulator of Cell-Cycle-Dependent Cross-Band Formation

To characterize the molecular mechanism of cross-band assembly, we determined the abundance of the Stp proteins over the course of the *Caulobacter* cell cycle. Each of the proteins was only barely detectable in swarmer cells but started to accumulate gradually after the swarmer-to-stalked-cell transition, with a distinct peak at the late predivisional stage

(Figure 4A). This pattern correlates well with the cell-cycle-expression patterns of *stpA*, *stpB* and *stpD* determined previously by global transcriptome analysis (McGrath et al., 2007), suggesting that synthesis of the Stp complex may largely be regulated at the transcriptional level. Consistent with this notion, continuous expression of *stpA* from an inducible promoter in a Δ*stpA* background abolished the observed fluctuations in StpA protein levels (data not shown). To investigate whether the cell-cycle-dependent accumulation of the four Stp proteins in fact correlated with the appearance of cross-bands, we monitored synchronously growing cells producing a StpB-mCherry fusion from the native *stpB* promoter (Figure 4B). In line with the observed abundance patterns, no fluorescence was observed in swarmer cells. However, polar StpB-mCherry foci became detectable once the cells had progressed halfway through the cell cycle. Furthermore, stalked cells consistently displayed a second StpB-mCherry focus after passing through an additional cell cycle (data not shown), indicating that the Stp proteins assemble in a cell-cycle-dependent manner. Notably, the intensity of the fluorescent foci increased over time, suggesting a gradual maturation of the complexes.

Next, we examined the order of Stp complex assembly. To this end, we engineered xylose-inducible fluorescent protein fusions to StpA–D and examined the localization pattern of each fusion in cells lacking either single or multiple Stp proteins (Figure 4C). StpB, StpC, and StpD were all mislocalized in a Δ*stpA* background, demonstrating that StpA provides a scaffold necessary for Stp complex formation. StpC localization further depended on the presence of StpB. Occasionally, we observed single StpB-mCherry or StpC-mCherry foci in Δ*stpA* or Δ*stpB* cells, respectively. However, these cells also showed occasional fluorescent dots within the cell body, suggesting that these foci likely represent protein aggregates that were accidentally inserted into the growing stalk. The localization hierarchy deduced from these analyses (Figure 4D) was corroborated by time-lapse microscopy of cells that coproduced StpD-GFP and mCherry-labeled derivatives of StpA, StpB, or StpC (Movies S2, S3, and S4). StpD-GFP consistently localized to the stalked pole significantly later than StpA-mCherry but earlier than StpC-mCherry. The temporal order of StpB and StpD recruitment could not be unambiguously resolved, suggesting that StpA independently and concurrently recruits both StpB and StpD to the nascent Stp complex.

A key role of StpA in cross-band formation is also supported by overexpression experiments. We noticed that cells carrying a plasmid with an additional copy of *stpAB* under the control of the P_{xyl} promoter displayed considerably more cross-bands, even in the absence of inducer (Figure 4E). This effect likely resulted from the elevated production of StpA and StpB due to leaky expression of the plasmid-borne genes (Figure S4C). Interestingly, induction of *stpAB* overexpression dramatically reduced cellular fitness (Figure S4D), accompanied by the formation of slender, elongated cells with short or misshapen stalks (data not shown). ECT analysis of StpAB-overproducing cells revealed that the stalks contained massive helical densities lining the periplasmic face of the inner membrane, supporting the idea that the Stp proteins assemble spontaneously into high-molecular weight structures (Figures 4F and S4E and Movie S5). These helical arrays did not extend into the cytoplasm or the outer membrane, consistent with the finding that StpB and the C-terminal region of StpA form a plasma membrane-associated periplasmic complex (Figure 2). The reason for the observed growth disadvantage is unclear. However, in many tomograms, the cytoplasmic membrane at the stalked pole was covered by an extensive layer of electron-dense material (Figure S4E). These structures may be related to the accumulation of StpAB and interfere with the function of polar protein complexes involved in the regulation of *Caulobacter* development.

To dissect the mechanism of Stp complex formation, we individually expressed *stpA-mCherry* and *stpB-mCherry* fusions integrated at the chromosomal P_{xyl} locus in an otherwise wild-type background and compared the number of fluorescent foci per micrometer stalk in cells after growth in low-phosphate medium. Importantly, induction of *stpA-mCherry*, but not *stpB-mCherry*, was sufficient to significantly increase the frequency of Stp complexes (Figure 4G). Cross-band assembly thus appears to be stimulated by StpA in a concentration-dependent, nucleation-like process.

The central importance of StpA in Stp complex assembly raises the question of how StpA itself is recruited to the stalked pole. Although the underlying mechanism still needs to be determined, we can exclude the involvement of several known polarly localized proteins, including the cell polarity determinant DivJ, the pole-organizing protein PopZ, the stalk-specific protein StpX, the penicillin-binding protein PpbC, and the scaffolding proteins BacA and BacB (Curtis and Brun, 2010; Hughes et al., 2010; Kühn et al., 2010) (Figure S4F).

Cross-Bands Are Nonspecific Barriers to Protein Diffusion

To test whether cross-bands were responsible for the observed compartmentalization of *Caulobacter* cells, we compared the mobility of a soluble periplasmic red fluorescent protein (TAT-tdimer2) in the wild-type and a StpAB-deficient mutant by using FLIP analysis (Figure 5A). In both strains, diffuse red fluorescence was detected throughout the stalk and the cell body periplasm prior to photobleaching. When wild-type cells were exposed to a laser pulse focused onto the stalk-distal pole, TAT-tdimer2 fluorescence was completely bleached within the cell body. The bleached region extended to the cross-band closest to the stalk base and did not recover any fluorescence within a 10 min interval. In about 20% of the cells (n = 20), TAT-tdimer2 fluorescence decreased up to the second cross-band, indicating that cross-band assembly may still have been in progress at the time of the bleaching event (data not shown). In contrast, when the same experiment was performed on StpAB-deficient cells, TAT-tdimer2 was completely bleached throughout the cell, including the stalk. Thus, periplasmic protein diffusion is no longer restricted in the absence of cross-bands. Notably, in a Δ*stpCD* mutant, which still forms electron-dense cross-band structures (Figure S3A), TAT-tdimer2 was only partly compartmentalized. Approximately 50% of the cells (n = 122) lost fluorescence in the unbleached region during a 10 min recovery period (Figure S5A), indicating that StpC and StpD are critical for tightening the diffusion barrier.

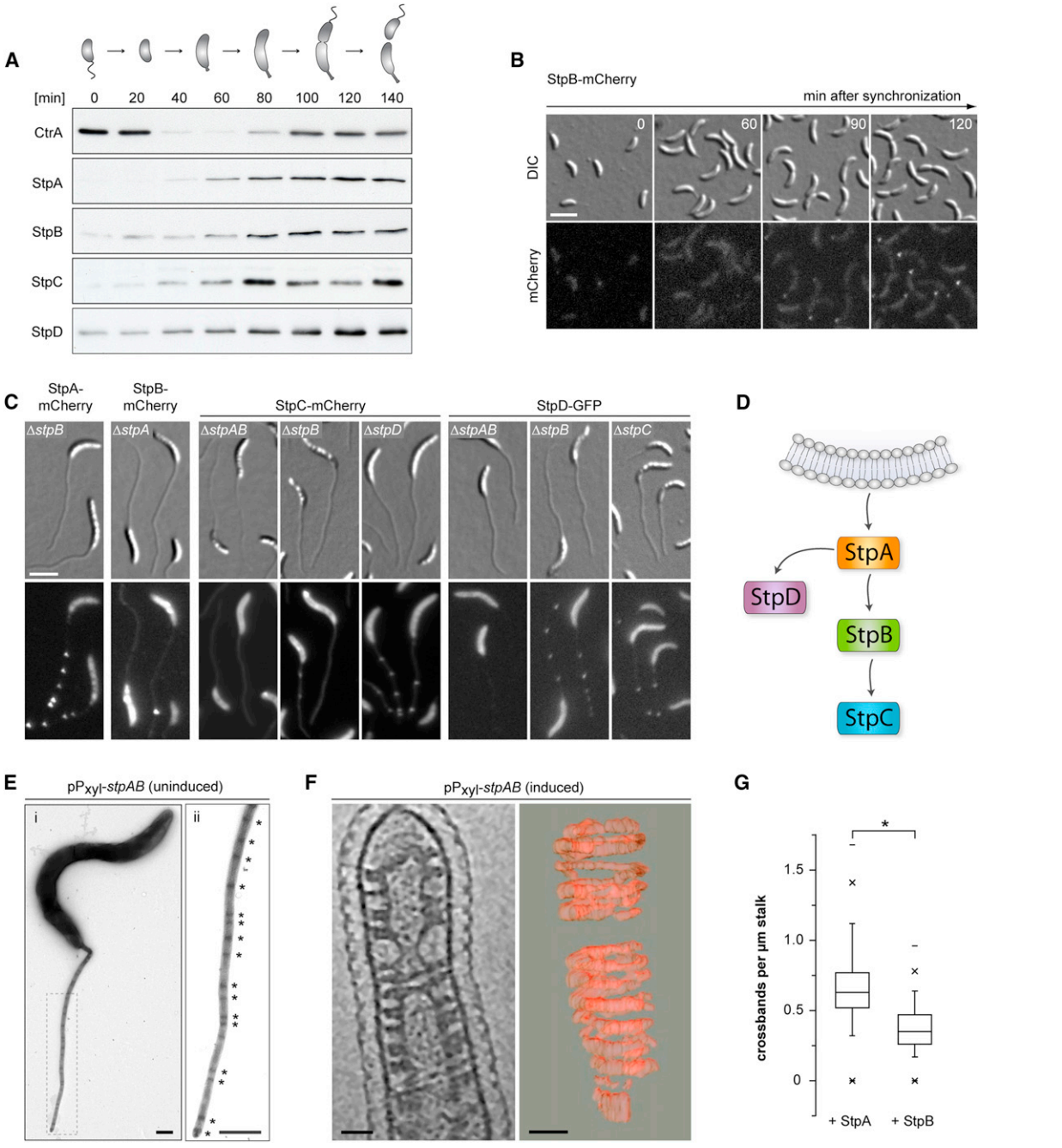

Figure 4. Cross-band Synthesis is Cell Cycle Dependent and Relies on Hierarchal Self-Assembly of the Stp Proteins

(A) Western blot analysis of Stp protein levels during the cell cycle. Swarmer cells of SS233 (*stpB*::stpB-*His*), SS247 (*stpC*::*stpC-His*) and SS244 (*stpD*::*stpD-His*) were grown in M2G. Samples were taken from the culture in 20 min intervals and probed with anti-CtrA, anti-StpA and anti-His antiserum. The schematic illustrates the morphology of *Caulobacter* cells at different stages of the cell cycle.

(B) Timecourse microscopy of StpB-mCherry localization, starting with isolated swarmer cells of SS160 (*stpB-mcherry*). Cells were grown in M2G. Scale bar, 3 μm.

(C) Localization hierarchy of the Stp proteins. Xylose-inducible fluorescent protein fusions to StpA, StpB, StpC, and StpD were analyzed in the indicated strain backgrounds (SS141, SS142, SS234, SS236, SS240, SS263, SS264, SS265). Cells were grown in $M2G^{-P}$ and induced for 24 hr with 0.3% xylose. Scale bar, 3 μm.

(D) Schematic illustrating the order of StpABCD complex assembly.

(E) Stalk ultrastructure of cells carrying an inducible copy of *stpAB* on a multicopy plasmid (SS214). Cells were cultivated in $M2G^{-P}$ in the absence of inducer, negatively contrasted with uranyl acetate, and imaged by transmission electron microscopy. The dashed rectangle in (i) indicates the region magnified in (ii). Asterisks indicate cross-bands. Scale bars, 500 nm. A strain carrying the empty plasmid (SS258) showed the wild-type frequency of cross-bands (data not shown).

We then determined whether cross-bands also compartmentalize the inner and outer membrane. For this purpose, FLIP analysis was performed on wild-type and Δ*stpAB* mutant cells producing mCherry fusions to the inner-membrane type II secretion protein GspG, the outer-membrane TonB-dependent receptor MalA (Neugebauer et al., 2005) and the outer-membrane lipoprotein ElpS (Le Blastier et al., 2010) (Figure S5E). In the wild-type background, fluorescence was only bleached in a defined subregion of the cell and did not show any recovery within a 10 min period following the bleaching event ($n > 30$ per strain). The Δ*stpAB* mutant, by contrast, showed no sign of compartmentalization for any of the proteins investigated ($n > 79$ per strain). Cross-bands thus act as general diffusion barriers that restrict the mobility of proteins in all layers of the cell envelope.

Next, we investigated how proteins can enter the stalk despite the presence of diffusion barriers. Our analyses showed that fluorescently labeled envelope proteins are distributed throughout the stalk when induced concomitantly with the onset of stalk growth (Figures 5A and S5E). Because cross-bands are inserted at intervals, diffusible proteins are likely to be trapped randomly in intrastalk compartments during stalk elongation. To test this hypothesis, we first grew cells synthesizing a xylose-inducible PstS-mCherry, GspG-mCherry or ElpS-mCherry fusion in low-phosphate medium lacking inducer to stimulate stalk elongation. Subsequently, synthesis of the fusion proteins was induced, and images were taken after an additional growth period (Figure 5B). In the wild-type background, the newly produced proteins only entered the stalk up to the newest cross-band. Moreover, they were occasionally trapped in the compartment formed by the two proximal cross-bands whenever a new Stp complex had assembled during the time of induction. In cross-band-deficient cells, by contrast, the fusions were able to diffuse freely throughout the entire cell envelope including the stalk. These results indicate that the timing of synthesis determines whether an envelope protein localizes to the stalk, with diffusion barriers helping to retain newly produced proteins in the cell body.

ECT analysis suggested that cross-bands might also compartmentalize the stalk cytoplasm (Figure 3A and Movie S1). However, consistent with the reported absence of cytoplasmic proteins in the stalk (Ireland et al., 2002; Wagner et al., 2006), we observed that the fluorescent protein YFP remained excluded from the stalk even in a Δ*stpAB* background (data not shown). To probe for stalk core compartmentalization, we therefore took advantage of the stalk-specific bitopic inner membrane protein StpX. Previously, StpX was shown to be immobile near the stalk base but mobile in stalk regions distal to the cell body (Hughes et al., 2010). We found that the spatial boundary between the immobile and mobile subpopulations consistently (100%; $n > 30$) coincided with the newest cross-band (Figure 5C). In contrast, StpX-GFP was largely immobile in barrier-deficient cells (Figure S5B). The mobile fraction was proposed to result from posttranslational processing of StpX (Hughes et al., 2010). Indeed, whereas StpX accumulated as a dominant short fragment in wild-type cells, this fragment was undetectable in StpAB-deficient cells (Figure 5D). The processed form presumably results from cleavage within the cytoplasmic domain of StpX (Figures 5D, S5C and S5D). Since the cleaved C-terminal domain is soluble (Hughes et al., 2010), the apparent mobility of StpX-GFP in wild-type cells is likely explained by the release of a GFP-containing fragment into the cytoplasm of intrastalk compartments, where its diffusion is constrained by cross-bands. Although the function of StpX and the nature of its processing are still unclear, these data demonstrate that diffusion barriers create intrastalk compartments that differ from the cell body in protein composition and/or activity.

Protein Diffusion Barriers Are Critical for Bacterial Fitness

Upon prolonged phosphate starvation, the stalk can account for the majority of the periplasmic volume and of the inner and outer membrane areas. Because cross-bands retain newly synthesized envelope proteins in the cell body (Figures 5A and 5B), they should allow faster protein accumulation during periods of protein upregulation. To test this hypothesis, we monitored the accumulation of a xylose-inducible PstS-mCherry fusion in the cell body periplasm of wild-type and StpAB-deficient cells after addition of the inducer (Figure 6A). Cells deficient in diffusion barriers showed a delay in PstS-mCherry accumulation of 22.4 ± 0.8 min compared to compartmentalized cells. Thus, a lack of diffusion barriers increases the effective periplasmic volume, necessitating a higher production of periplasmic proteins to reach final steady-state levels.

To test for a possible selective advantage of diffusion barriers, we performed competitive growth experiments. Wild-type and Δ*stpAB* mutant cells, labeled with distinct fluorescent proteins, were first grown individually in low-phosphate medium and then mixed at equal ratios. After transfer of the mixed culture to phosphate-rich medium and cultivation to late-exponential phase, the fraction of wild-type cells was determined by fluorescence microscopy ($n > 1{,}000$). We consistently found that wild-type cells outcompeted barrier-deficient cells in recovery from phosphate starvation. Because the growth rates of the two strains are equal in phosphate-rich medium (Figure S6A), we reasoned that the competitive advantage of wild-type cells stems from a delay in the onset of cell division in the noncompartmentalized Δ*stpAB* cells. The delay calculated for Δ*stpAB* cells relative to the wild-type was 1.39 ± 0.25 hr (Figures 6B, S6B and S6C). We additionally performed growth competition experiments by using Δ*stpCD* mutant cells, which display leaky diffusion barriers and are thus only partially compartmentalized

(F) Visualization and 3D-reconstruction of helical StpAB assemblies. Cells carrying a plasmid-encoded copy of *stpAB* under the control of P_{xyl} (SS214) were precultured in PYE, grown in $M2G^{-P}$ containing 0.3% xylose, and analyzed by ECT. Shown is a section through a representative tomogram of a stalk (left) and a 3D reconstruction of the helical assemblies induced by StpAB overproduction (right). Scale bars, 50 nm.

(G) Constitutive production of StpA increases the frequency of cross-bands. Cells of strain SW33 (P_{xyl}::P_{xyl}-*stpA-mcherry*) and SW30 (P_{xyl}::P_{xyl}-*stpB-mcherry*) were grown in $M2G^{-P}$ with 0.3% xylose for 24 hr and imaged by fluorescence microscopy. The number of fluorescent foci per μm stalk was determined for cells of SW30 ($n = 120$) and SW33 ($n = 194$) (*$p < 0.05$, t test). Box plots were drawn as described in Figure 3C. See also Figure S4.

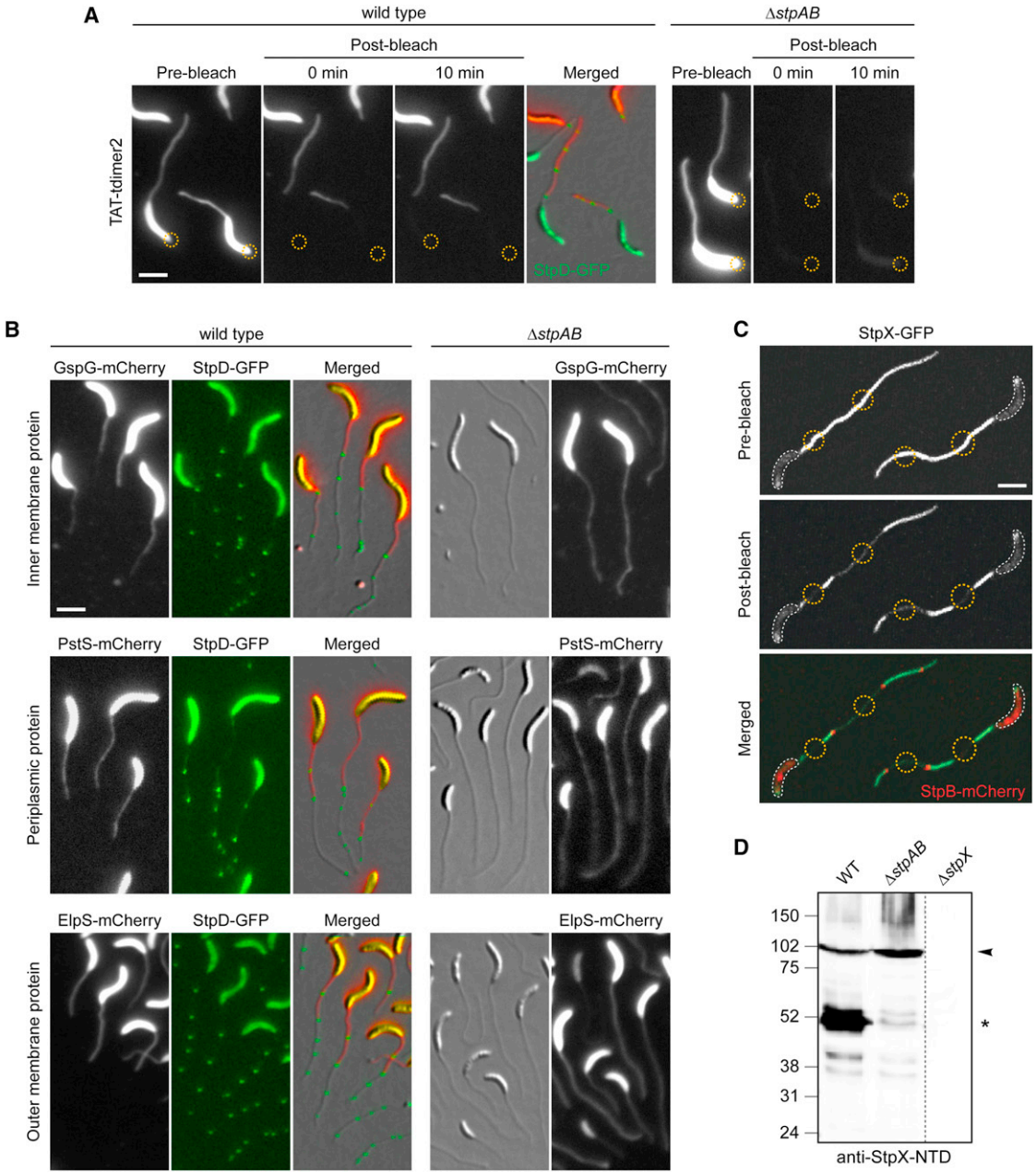

Figure 5. Cross-Bands Serve as Protein Diffusion Barriers

(A) Analysis of the compartmentalization of soluble and periplasmic red fluorescent protein (TAT-tdimer2) with FLIP. Cells of strain SS269 (*stpD::stpD-gfp* pP_{xyl}-*TAT-tdimer2*) and SS216 (Δ*stpAB* pP_{xyl}-*TAT-tdimer2*) were cultured in $M2G^{-P}$ containing 0.3% xylose for 24 hr. Cells were mounted on an agarose pad and exposed to a laser pulse in the regions indicated by a yellow circle. Scale bar, 3 μm.

(B) Cross-bands compartmentalize periplasmic, inner- and outer membrane proteins. Cells of strains SS277 (*stpD::stpD-gfp* P_{xyl}-*gspG-mcherry*), SS272 (Δ*stpAB* P_{xyl}::P_{xyl}-*gspG-mcherry*), SS299 (*stpD::stpD-gfp* P_{xyl}::P_{xyl}-*pstS-mcherry*), SS302 (Δ*stpAB* P_{xyl}::P_{xyl}-*pstS-mcherry*), SS283 (*stpD::stpD-gfp* P_{xyl}::P_{xyl}-*elpS-mcherry*), and SS284 (Δ*stpAB* P_{xyl}::P_{xyl}-*elpS-mcherry*) were first grown in $M2G^{-P}$ for 36 hr and then induced with 0.3% xylose for 11–13 hr. Scale bar, 3 μm.

(C) StpX-GFP mobility requires compartmentalization of the stalk from the cell body by the newest cross-band. Cells of strain YB5058 (*stpX::stpX-gfp* P_{xyl}::P_{xyl}-*stpB-mcherry)* were grown in HIGG-30 μM phosphate containing 0.3% xylose and mounted on an agarose pad. First, StpB-mCherry fluorescence was imaged to identify regions of interest (yellow circles). Then, these regions were simultaneously bleached for 50 s, followed by the acquisition of a postbleach image. White lines outline the cell bodies. Scale bar, 3 μm.

(D) Cross-bands affect the processing of the stalk-specific protein StpX. Wild-type, Δ*stpAB* (SW51) and Δ*stpX* (YB5231) cells were grown to stationary phase in HIGG-30 μM phosphate and subjected to immunoblot analysis with an antibody raised against the N-terminal domain of StpX (anti-StpX-NTD). The full-length version of StpX is denoted by an arrowhead, the dominant short fragment by an asterisk. See also Figure S5.

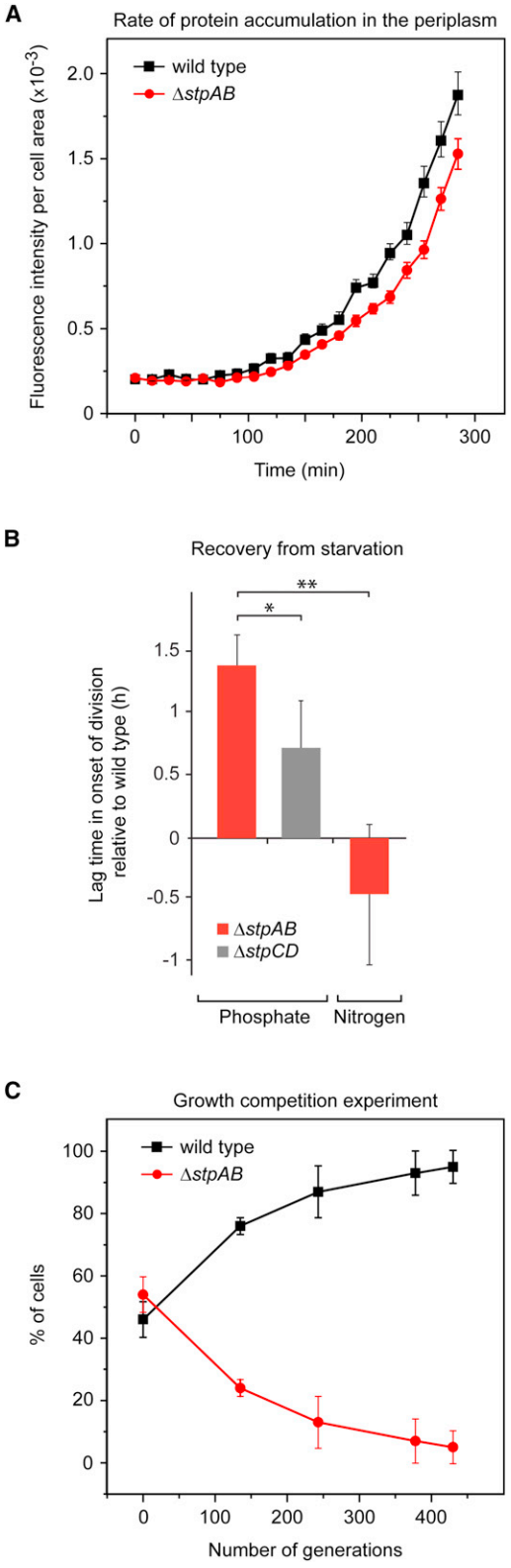

Figure 6. Diffusion Barriers Confer a Critical Fitness Advantage

(A) Rate of periplasmic accumulation of an inducible PstS-mCherry protein fusion in the wild-type (EK363) and Δ*stpAB* (EK389) background. Cells were grown in HIGG-30 μM phosphate with 0.3% glucose to induce long stalks while repressing the synthesis of PstS-mCherry. The cells were seeded on pads with 0.3% xylose, and PstS-mCherry accumulation was monitored by time-lapse microscopy. Mean fluorescence/cell body area was measured for ~300 cells per strain. Error bars = SD. Fitting the data to an exponential function and solving the equations in the exponential region (t = 165 to 255 min) for equal fluorescence intensities yielded a time difference in the accumulation of PstS-mCherry of 22.4 (±0.8) min.

(B) Competitive growth of wild-type and diffusion barrier-deficient cells. To analyze the effect of diffusion barriers on the rate of recovery from nutrient starvation, wild-type, Δ*stpAB* and Δ*stpCD* cells were differentially labeled with the fluorescent proteins YFP (EK392, EK417, EK486) or mCherry (EK416, EK393, EK487) and starved for either phosphate or nitrogen. Mutant and wild-type cells were combined at equal ratios, transferred to nutrient-replete medium and grown to late-exponential phase. More than 1,000 cells were analyzed by fluorescence microscopy before and after recovery to determine shifts in the relative composition of the cultures. The differentials were then used to calculate the lag in the onset of cell division (see Figure S6B). Values represent the average of four experiments, including two in which the fluorescent marker was switched (error bars = SD; *$p < 0.02$; **$p < 0.002$).

(C) Wild-type cells outcompete a diffusion barrier-deficient mutant. Wild-type and Δ*stpAB* cells (SW51) were grown in PYE and mixed at equal optical densities. Mixed cultures (n = 5) were repeatedly diluted into fresh PYE and cultured to stationary phase. At the indicated time points, cells were withdrawn and spread on PYE agar. The ratio of wild-type and barrier-deficient cells was determined by colony PCR. Error bars show SD (n ~450). See also Figure S6.

(see Figure S5A). Whereas cells deficient in StpCD were still outcompeted by wild-type cells, the calculated lag in restarting cell division was significantly shorter (0.72 ± 0.38 hr, $p < 0.02$) (Figure 6B). These data support the hypothesis that diffusion barriers provide a fitness advantage by reducing the effective envelope area and periplasmic volume of the cell and thus accelerating the rate of new protein accumulation.

To provide additional evidence that the effective cell envelope volume is critical for fitness, we asked whether the observed competition advantage of wild-type cells was directly linked to stalk length. Given the lack of true stalk-less mutants, we took advantage of the fact that nitrogen-limiting growth conditions do not stimulate stalk elongation (Figure S6D), yielding relatively similar envelope volumes for wild-type and diffusion barrier-deficient (Δ*stpAB*) cells. As expected, we found that wild-type cells had no measurable growth advantage over the mutant strain after transfer from nitrogen-limited to nitrogen-rich medium (Figure 6B), consistent with a positive effect of volume reduction on cellular fitness.

The Stp complex is synthesized in both starvation and nutrient-rich conditions (see Figure 4), suggesting that subcellular compartmentalization is critical even when only short stalks are produced. Because short-term competition assays may not be sensitive enough to detect small fitness differences, we carried out long-term experiments with untagged cells that were fully (wild-type), partially (Δ*stpCD*), or not (Δ*stpAB*) compartmentalized. Mixed cultures initially containing an equal ratio of wild-type and Δ*stpAB* or Δ*stpCD* cells were repeatedly grown to stationary phase and then rediluted into fresh rich medium for approximately 450 generations. Monitoring changes in the relative abundance of the respective strains over time, we observed that wild-type cells efficiently outcompeted a mutant with defective diffusion barriers (Figures 6C and S6E). The

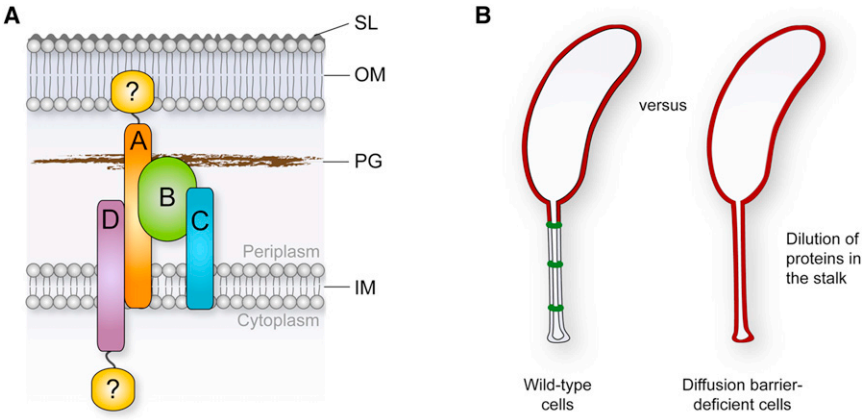

Figure 7. Model for Diffusion Barrier Formation and Function

(A) Diffusion barrier assembly can be envisioned as a nucleation-like process in which StpA (orange) and StpB (green) form the basic scaffold. StpC (blue) and StpD (purple) are accessory components that are required to seal the diffusion barrier. Potential unidentified components of the complex that may establish a connection to the outer membrane or assemble at the cytoplasmic face of the inner membrane are depicted in yellow.

(B) The synthesis of diffusion barriers minimizes the effective volume of the periplasmic space and reduces the physiologically active membrane surface area. In the absence of diffusion barriers, newly synthesized proteins that are targeted to the cell envelope are constantly diluted due to diffusion into the stalk extension.

selection coefficients (Lang et al., 2009) calculated for the Δ*stpAB* and Δ*stpCD* strains were −0.7% and −0.4%, respectively. The value obtained for StpAB-deficient cells corresponds to a difference in doubling times of only 4.6%. This delay is too small to be resolved by short-term growth analyses but provides a critical advantage over longer time scales. Collectively, our results thus show that diffusion barriers make an important general contribution to cellular fitness.

DISCUSSION

Intracellular compartmentalization by protein-mediated diffusion barriers has previously been thought to be a characteristic of eukaryotic cells. In this study, we show that general protein diffusion barriers, analogous to those reported for cilia or neuronal axons (Chih et al., 2012; Nakada et al., 2003), also exist in prokaryotes. These structures are functionally and structurally different from bacterial microcompartments (Murat et al., 2010) because they do not only encapsulate a distinct set of functionally related enzymes but rather divide the whole cell into physiologically distinct domains. Unlike in eukaryotic cells, these diffusion barriers not only laterally compartmentalize cellular membranes but also limit the free diffusion of soluble proteins, thereby providing a significant fitness advantage. Diffusion barrier formation in *Caulobacter* therefore represents a thus far unrecognized mechanism to optimize the growth of a prokaryote by restricting protein mobility within the cell.

Timing and Assembly of the StpABCD Diffusion Barrier Complex

The formation of the StpABCD diffusion barrier complex is coordinated with the developmental program and occurs in the second half of the cell cycle, consistent with earlier reports on the temporal appearance of cross-bands as visualized by electron microscopy (Poindexter and Staley, 1996; Staley and Jordan, 1973). Upon synthesis, the Stp proteins are targeted to the stalked pole in a hierarchal order, with StpA taking the top position in the localization hierarchy. The cellular abundance of StpA appears to be the rate-limiting factor in de novo diffusion barrier formation because the frequency of cross-bands scales with the expression level of the *stpA* gene. Thus, diffusion barrier assembly may be triggered as soon as a critical number of StpA molecules have accumulated in the cell. After the recruitment of StpB, which is also essential for the formation of microscopically discernible cross-band structures, StpC and StpD are incorporated to seal the diffusion barrier complex (Figure 7A). Notably, overproduction of StpAB leads to the formation of large helical assemblies in the stalk periplasm (Figure 4F and Movie S5). The two proteins thus self-assemble to form a membrane-associated macromolecular complex (Figure 2) that provides the basic scaffold for diffusion barrier formation.

The establishment of diffusion barriers is uncoupled from the cell cycle when cells are grown in low-phosphate medium, a condition that causes a general arrest of cell-cycle progression but leads to constitutive elongation of the stalk (Gonin et al., 2000). Despite the lack of developmental cues, such as DNA replication and cell division, the growing stalk continues to be segmented by cross-bands, albeit at somewhat irregular intervals. The precise mechanism that controls the timing of Stp complex formation in these conditions remains unclear. However, it is conceivable that nucleation of a cross-band leads to a transient drop in the cellular concentration of StpA, which prevents formation of another complex until StpA levels rise again above a critical threshold level.

If StpA is required for recruiting the remaining Stp proteins to the stalk base, what targets StpA to the stalked pole in the first place? Thus far, we have been unable to identify a localization factor upstream of StpA. However, formation of the stalk creates a region of positive membrane curvature at the stalk base, which could be specifically recognized by StpA, reminiscent of the mechanism described for the bacterial proteins SpoVM and DivIVA (Ramamurthi et al., 2009).

Our data strongly suggest that cross-bands are high-molecular weight protein complexes rather than discs made of peptidoglycan, as proposed previously (Jones and Schmidt, 1973; Schmidt, 1973). In support of this hypothesis and consistent with the observation that FtsZ does not localize to the stalked pole (Thanbichler and Shapiro, 2006), cross-band formation was found to be independent of FtsZ-mediated peptidoglycan synthesis. Moreover, whereas the peptidoglycan biosynthetic apparatus is localized to the periplasmic space, cross-bands

extend on both sides of the cytoplasmic membrane, reaching from the outer membrane to the cytoplasmic core (Figure 3A). Most importantly, however, cross-bands are not detectable in purified murein sacculi, although they are significantly thicker than the cellular peptidoglycan layer (Gan et al., 2008; A.B. and G.J.J., unpublished data). The previous observation that fewer cross-bands are detectable upon treatment of stalks with lysozyme is thus likely explained by an indirect, stabilizing effect of the cell wall on StpABCD complex assembly.

Physiological Significance of Protein Diffusion Barriers in Stalked Bacteria

Caulobacter thrives in oligotrophic aquatic environments, where inorganic phosphorus commonly represents the limiting nutrient (Paerl, 1982). The *Caulobacter* stalk elongates in response to phosphate starvation, leading to the hypothesis that it acts as a "nutrient scavenging antenna" (Gonin et al., 2000; Schmidt and Stanier, 1966; Wagner et al., 2006). The presence of diffusion barriers, however, challenges the currently held model that phosphate-bound PstS diffuses through the stalk to deliver its cargo to the PstCAB inner-membrane transporter in the cell body (Wagner et al., 2006). However, it is possible that previous experiments have simply failed to detect the PstCAB complex in the stalk, opening the possibility that PstS-bound phosphate is targeted immediately to the stalk cytoplasm. Although the diffusion of proteins is restricted in the stalk, small molecules such as phosphate may be able to pass cross-bands and then use the stalk core to travel to the cell body.

Regardless of a possible role in phosphate uptake, the stalk may predominantly function to spatially separate the cell body from the point of holdfast attachment. Elevation of the cell body may provide various selective advantages such as the ability to rise above an existing biofilm or to expose the immobilized cell to bulk nutrients (Wagner and Brun, 2007). Because the stalk is a true extension of the cell envelope, lengthening of this polar structure leads to an increase in the membrane surface area and periplasmic volume. While under optimal growth conditions, the stalk periplasm only accounts for ~10% of the total periplasmic volume, this value can increase considerably in response to phosphate starvation. We have demonstrated that periplasmic, inner and outer membrane proteins can diffuse freely throughout the cell in the absence of diffusion barriers, so that newly synthesized proteins are constantly diluted in the stalk extension (Figure 7B). Notably, membrane proteins make up approximately 20% to 30% of the total protein in a bacterial cell (Wallin and von Heijne, 1998). Diffusion barrier formation is therefore an efficient mechanism to minimize the effective area/volume of the cell envelope and, thus, reduce the energetic cost of establishing or maintaining a pool of physiologically active envelope proteins. Moreover, physiological compartmentalization could facilitate faster adaptation to sudden environmental or developmental cues that require the induction and accumulation of a different set of envelope proteins to ensure overall fitness. The benefit of such diffusion barriers may be relatively widespread as cross-bands have been identified in a range of stalked bacteria. Notably, the StpB homolog of the prosthecate species *Asticcacaulis excentricus* displays a similar stalk localization pattern as *Caulobacter* StpB (Figure S2B), indicating that cross-band formation is also mediated by the Stp complex in these organisms.

Collectively, we have identified and functionally characterized a previously unrecognized protein compartmentalization mechanism that relies on the assembly of at least four proteins into a diffusion barrier complex. Structural analyses may provide insights into the precise mechanism underlying the self-assembly and subcellular localization of this structure. Our findings open the possibility that diffusion barriers could exist in a wider range of prokaryotes, providing a stimulating framework for future studies.

EXPERIMENTAL PROCEDURES

Bacterial Strains, Plasmids, and Growth Conditions

The strains and plasmids used in this study are described in Tables S1, S2, and S3. *Caulobacter* wild-type strain CB15N and its derivatives were grown at 28°C in peptone-yeast-extract (PYE) medium (Poindexter, 1964) or M2-glucose (M2G) minimal medium. To achieve stalk elongation in response to phosphate starvation, stationary cells were diluted 1:20 in $M2G^{-P}$ (Kühn et al., 2010) containing 3.9 mM KCl and cultured for additional 24 hr. Alternatively, cells were directly grown in Hutner imidazole-buffered glucose-glutamate (HIGG) medium containing 30 μM phosphate (Poindexter, 1978). Cell synchronization and growth competition experiments are detailed in the Extended Experimental Procedures.

Immunoblot Analysis

Immunoblot analysis was performed as described previously (Thanbichler and Shapiro, 2006). Details on the antibodies used are given in the Extended Experimental Procedures.

Cell Fractionation and Coimmunoprecipitation Analysis

Biochemical fractionation of cells was performed as described previously (Möll et al., 2010). For coimmunoprecipitation analysis, StpB-His was isolated from dodecyl maltoside-treated cell extracts with anti-His affinity beads and analyzed for interactors with immunoblot analysis or mass spectrometry. Experimental details are given in the Extended Experimental Procedures.

Fluorescence Microscopy

For light microscopy, cells were spotted onto pads made of 1% agarose (for still images) or 1% agarose in M2G medium (for time-lapse analyses). Details on the fluorescence microscopy and FRAP/FLIP setups are given in the Extended Experimental Procedures.

Electron Microscopy

The analysis of negatively stained *Caulobacter* cells by transmission electron microscopy is detailed in the Extended Experimental Procedures.

Electron cryotomography (ECT) was performed as described (Möll et al., 2010). Correlated fluorescence light microscopy (FLM) combined with ECT was essentially carried out as reported previously (Ingerson-Mahar et al., 2010), with the exception that cells were immobilized on C flat 2/2 London finder copper TEM grids with a ~40 nm thick holey carbon coat (Protochips Inc., Raleigh, NC, USA), which were treated with 5 μl of 1 mg/ml sterile-filtered poly-L-lysine (Sigma, P1524) before use. The correlative analysis was performed manually with Photoshop software (Adobe Systems). The prominent holes in the carbon foil together with the cell body and stalk densities were sufficient to unambiguously overlay the FLM images and the ECT slices. Details on the tools used for image analysis are given in the Extended Experimental Procedures.

SUPPLEMENTAL INFORMATION

Supplemental Information includes Extended Experimental Procedures, six figures, four tables, five movies and can be found with this article online at http://dx.doi.org/10.1016/j.cell.2012.10.046.

ACKNOWLEDGMENTS

We thank Stephanie Wick for excellent technical assistance; Nikolay Ouzounov for helpful discussions; Juliane Kühn, Patrick Viollier, and Grant Bowman for providing plasmids and strains; and Sarah Cheng for help with image segmentation. This work was supported by funds from the Max Planck Society to M.T., a Young Investigator Grant (RGY0069/2008-C) from the Human Frontier Science Program to Z.G. and M.T., a National Institutes of Health (NIH) Director's New Innovator Award (DP2OD004389) to Z.G., an NRSA postdoctoral fellowship (F32GM906842) from the National Institute of General Medical Sciences to E.A.K., NIH grant GM51986 to Y.V.B, and NIH grant RO1 GM094800B to G.J.J.

Received: March 19, 2012
Revised: July 24, 2012
Accepted: October 14, 2012
Published online: November 29, 2012

REFERENCES

Blatch, G.L., and Lässle, M. (1999). The tetratricopeptide repeat: a structural motif mediating protein-protein interactions. Bioessays *21*, 932–939.

Caudron, F., and Barral, Y. (2009). Septins and the lateral compartmentalization of eukaryotic membranes. Dev. Cell *16*, 493–506.

Chih, B., Liu, P., Chinn, Y., Chalouni, C., Komuves, L.G., Hass, P.E., Sandoval, W., and Peterson, A.S. (2012). A ciliopathy complex at the transition zone protects the cilia as a privileged membrane domain. Nat. Cell Biol. *14*, 61–72.

Curtis, P.D., and Brun, Y.V. (2010). Getting in the loop: regulation of development in *Caulobacter crescentus*. Microbiol. Mol. Biol. Rev. *74*, 13–41.

Divakaruni, A.V., Baida, C., White, C.L., and Gober, J.W. (2007). The cell shape proteins MreB and MreC control cell morphogenesis by positioning cell wall synthetic complexes. Mol. Microbiol. *66*, 174–188.

Gan, L., Chen, S., and Jensen, G.J. (2008). Molecular organization of Gram-negative peptidoglycan. Proc. Natl. Acad. Sci. USA *105*, 18953–18957.

Gonin, M., Quardokus, E.M., O'Donnol, D., Maddock, J., and Brun, Y.V. (2000). Regulation of stalk elongation by phosphate in *Caulobacter crescentus*. J. Bacteriol. *182*, 337–347.

Hughes, H.V., Huitema, E., Pritchard, S., Keiler, K.C., Brun, Y.V., and Viollier, P.H. (2010). Protein localization and dynamics within a bacterial organelle. Proc. Natl. Acad. Sci. USA *107*, 5599–5604.

Ingerson-Mahar, M., Briegel, A., Werner, J.N., Jensen, G.J., and Gitai, Z. (2010). The metabolic enzyme CTP synthase forms cytoskeletal filaments. Nat. Cell Biol. *12*, 739–746.

Ireland, M.M., Karty, J.A., Quardokus, E.M., Reilly, J.P., and Brun, Y.V. (2002). Proteomic analysis of the *Caulobacter crescentus* stalk indicates competence for nutrient uptake. Mol. Microbiol. *45*, 1029–1041.

Jones, H.C., and Schmidt, J.M. (1973). Ultrastructural study of crossbands occurring in the stalks of *Caulobacter crescentus*. J. Bacteriol. *116*, 466–470.

Kühn, J., Briegel, A., Mörschel, E., Kahnt, J., Leser, K., Wick, S., Jensen, G.J., and Thanbichler, M. (2010). Bactofilins, a ubiquitous class of cytoskeletal proteins mediating polar localization of a cell wall synthase in *Caulobacter crescentus*. EMBO J. *29*, 327–339.

Lang, G.I., Murray, A.W., and Botstein, D. (2009). The cost of gene expression underlies a fitness trade-off in yeast. Proc. Natl. Acad. Sci. USA *106*, 5755–5760.

Le Blastier, S., Hamels, A., Cabeen, M., Schille, L., Tilquin, F., Dieu, M., Raes, M., and Matroule, J.Y. (2010). Phosphate starvation triggers production and secretion of an extracellular lipoprotein in *Caulobacter crescentus*. PLoS ONE *5*, e14198.

Marks, M.E., Castro-Rojas, C.M., Teiling, C., Du, L., Kapatral, V., Walunas, T.L., and Crosson, S. (2010). The genetic basis of laboratory adaptation in *Caulobacter crescentus*. J. Bacteriol. *192*, 3678–3688.

McGrath, P.T., Lee, H., Zhang, L., Iniesta, A.A., Hottes, A.K., Tan, M.H., Hillson, N.J., Hu, P., Shapiro, L., and McAdams, H.H. (2007). High-throughput identification of transcription start sites, conserved promoter motifs and predicted regulons. Nat. Biotechnol. *25*, 584–592.

Möll, A., Schlimpert, S., Briegel, A., Jensen, G.J., and Thanbichler, M. (2010). DipM, a new factor required for peptidoglycan remodelling during cell division in *Caulobacter crescentus*. Mol. Microbiol. *77*, 90–107.

Murat, D., Byrne, M., and Komeili, A. (2010). Cell biology of prokaryotic organelles. Cold Spring Harb. Perspect. Biol. *2*, a000422.

Nakada, C., Ritchie, K., Oba, Y., Nakamura, M., Hotta, Y., Iino, R., Kasai, R.S., Yamaguchi, K., Fujiwara, T., and Kusumi, A. (2003). Accumulation of anchored proteins forms membrane diffusion barriers during neuronal polarization. Nat. Cell Biol. *5*, 626–632.

Neugebauer, H., Herrmann, C., Kammer, W., Schwarz, G., Nordheim, A., and Braun, V. (2005). ExbBD-dependent transport of maltodextrins through the novel MalA protein across the outer membrane of *Caulobacter crescentus*. J. Bacteriol. *187*, 8300–8311.

Paerl, H.W. (1982). Factors limiting productivity of freshwater ecosystems. In Advances in microbial ecology, K.C. Marhal, ed. (New York: Plenum), pp. 75–110.

Poindexter, J.S. (1964). Biological Properties and Classification of the *Caulobacter* Group. Bacteriol. Rev. *28*, 231–295.

Poindexter, J.S. (1978). Selection for nonbuoyant morphological mutants of *Caulobacter crescentus*. J. Bacteriol. *135*, 1141–1145.

Poindexter, J.L.S., and Cohen-Bazire, G. (1964). Fine structure of stalked bacteria belonging to family *Caulobacteraceae*. J. Cell Biol. *23*, 587–607.

Poindexter, J.S., and Staley, J.T. (1996). *Caulobacter* and *Asticcacaulis* stalk bands as indicators of stalk age. J. Bacteriol. *178*, 3939–3948.

Ramamurthi, K.S., Lecuyer, S., Stone, H.A., and Losick, R. (2009). Geometric cue for protein localization in a bacterium. Science *323*, 1354–1357.

Schmidt, J.M. (1973). Effect of lysozyme on crossbands in stalks of *Caulobacter crescentus*. Arch. Mikrobiol. *89*, 33–40.

Schmidt, J.M., and Stanier, R.Y. (1966). The development of cellular stalks in bacteria. J. Cell Biol. *28*, 423–436.

Schmidt, J.M., and Swafford, J.R. (1975). Ultrastructure of crossbands in prosthecae of *Asticcacaulis* species. J. Bacteriol. *124*, 1601–1603.

Seitz, L.C., and Brun, Y.V. (1998). Genetic analysis of mecillinam-resistant mutants of *Caulobacter crescentus* deficient in stalk biosynthesis. J. Bacteriol. *180*, 5235–5239.

Smit, J., and Agabian, N. (1982). Cell surface patterning and morphogenesis: biogenesis of a periodic surface array during *Caulobacter* development. J. Cell Biol. *95*, 41–49.

Staley, J.T., and Jordan, T.L. (1973). Crossbands of *Caulobacter crescentus* stalks serve as indicators of cell age. Nature *246*, 155–156.

Thanbichler, M., and Shapiro, L. (2006). MipZ, a spatial regulator coordinating chromosome segregation with cell division in *Caulobacter*. Cell *126*, 147–162.

Wagner, J.K., and Brun, Y.V. (2007). Out on a limb: how the *Caulobacter* stalk can boost the study of bacterial cell shape. Mol. Microbiol. *64*, 28–33.

Wagner, J.K., Setayeshgar, S., Sharon, L.A., Reilly, J.P., and Brun, Y.V. (2006). A nutrient uptake role for bacterial cell envelope extensions. Proc. Natl. Acad. Sci. USA *103*, 11772–11777.

Wallin, E., and von Heijne, G. (1998). Genome-wide analysis of integral membrane proteins from eubacterial, archaean, and eukaryotic organisms. Protein Sci. *7*, 1029–1038.

EXTENDED EXPERIMENTAL PROCEDURES

Bacterial Strains and Plasmids

The bacterial strains and plasmids used in this study are listed in Tables S1, S2 and S3. Their construction is detailed in Tables S1 and S3, and the oligonucleotides used are listed in Table S4. All plasmids were verified by DNA sequencing. Gene replacement was performed by double homologous recombination using a two-step protocol based on the counter-selectable marker *sacB*. Proper integration of constructs into the *Caulobacter* chromosome was tested by colony PCR.

Growth Conditions and Synchronization

Caulobacter wild-type strain CB15N and its derivatives were grown at 28°C in peptone-yeast-extract (PYE) medium (Poindexter, 1964) or M2-glucose (M2G) minimal medium. To achieve stalk elongation in response to phosphate starvation, stationary cells were diluted 1:20 in $M2G^{-P}$ (Kühn et al., 2010) containing 3.9 mM KCl and cultured for additional 24 hr. Alternatively, cells were directly grown in Hutner imidazole-buffered glucose-glutamate (HIGG) medium containing 30 μM phosphate (Poindexter, 1978). To induce gene expression from the *xylX* promoter (P_{xyl}) (Meisenzahl et al., 1997), medium was supplemented with 0.1% or 0.3% D-xylose. *E. coli* strain TOP10 was used for general cloning purposes. Cells were grown at 37°C in Super Broth (Botstein et al., 1975). Antibiotics were added at the following concentrations (μg ml^{-1}; liquid/solid medium): spectinomycin (25/50), streptomycin (–/5), gentamicin (0.5/5), kanamycin (5/25), ampicillin (-/50) for *Caulobacter* and spectinomycin (50/100), kanamycin (30/50), chloramphenicol (20/30), tetracyline (12/12) for *E. coli*.

Synchronization of *Caulobacter* for microscopy and protein expression analysis was achieved by density gradient centrifugation using Percoll (Tsai and Alley, 2001) or Ludox AS-40 (Sigma-Aldrich) (Ely, 1991), respectively.

Growth Competition Experiments

For short-term competition assays, wild-type, Δ*stpAB* and Δ*stpCD* cells expressing xylose-inducible yellow (YFP) or red (mCherry) fluorescent protein (EK392, EK393, EK416, EK417, EK486, and EK487) were either starved for phosphate (HIGG-30 nM phosphate, 8.9 mM NH_4Cl) or nitrogen (HIGG-200 μM phosphate, 0.4 mM NH_4Cl) in the presence of 0.03% xylose for 3-4 days and mixed at equal optical densities. The exact ratio of wild-type to mutant cells was measured by counting ~1,000 cells by fluorescence microscopy. Cells were resuspended in recovery medium (HIGG-200 μM phosphate, 8.9 mM NH_4Cl) and grown with shaking to late-exponential phase (for 17 hr). The final cell ratio was measured by counting > 1,000 cells by fluorescence microscopy.

For long-term competition assays, mixtures of wild-type and Δ*stpAB* (SW51) or Δ*stpCD* cells (SS250) were repeatedly grown in PYE medium and diluted 1:500 into fresh medium once they had reached stationary phase. The ratio of wild-type to mutant cells was quantified by colony PCR, screening for the absence or presence of the respective mutations. The competition experiments were performed in quintuplicate (Δ*stpAB*) or triplicate (Δ*stpCD)* with independent starting cultures. At least 90 colonies were analyzed per culture and time point.

Immunoblot Analysis

A polyclonal anti-StpA antibody was raised by immunization of rabbits with the StpA-derived peptides 'YPPESPDSGVPHSDEA' (AA 299–314) and 'VSRPPRAAGERPQPRP' (AA 481–496) (Eurogentec). Immunoblot analysis was performed as described previously (Thanbichler and Shapiro, 2006) with anti-StpA, anti-CtrA (Domian et al., 1997), anti-His (Sigma-Aldrich, Germany), anti-GFP (Sigma-Aldrich, Germany), anti-RFP (Chen et al., 2005), anti-SpmX (Radhakrishnan et al., 2008) and anti-StpX (Hughes et al., 2010) rabbit antiserum at dilutions of 1:2,500 (StpA), 1:3,000 (His), 1:10,000 (CtrA, GFP, RFP) or 1:50,000 (SpmX, StpX).

Cell Fractionation Experiments

Biochemical fractionation of cells was performed as described previously (Möll et al., 2010). Cells were cultured in 80 ml PYE to an OD600 of 0.6 and harvested by centrifugation. Pellets were washed in 80 ml 0.2 M Tris-HCl (pH 8) and resuspended in 8 ml 60 mM Tris-HCl (pH 8) containing 0.2 M sucrose, 0.2 mM EDTA, 100 μg/ml PMSF, 5 μg/ml DNaseI and 10 mg/ml lysozyme. The cell suspension was incubated for 10 min at room temperature and frozen in liquid nitrogen. The cells were thawed on ice and lysed by sonication. Cell debris was removed by centrifugation for 10 min at 4,000 g. Subsequently, proteins were fractionated by ultracentrifugation at 100,000 g for 1 hr (4°C). Sedimented membrane proteins were washed in 1 volume 0.2 M Tris-HCl (pH 8) and resuspended in one volume 60 mM Tris-HCl (pH 8) containing 0.2 M sucrose. Protein samples were mixed with 2× SDS sample buffer and analyzed by immunoblotting.

Coimmunoprecipitation and Mass Spectrometric Analysis

Caulobacter strains CB15N (WT) and SS233 (*stpB::stpB*-His) were cultured in 1 l $M2G^{-P}$ for 12 hr. Proteins were crosslinked with 0.6% paraformaldehyde (in 1× PBS, pH 7.4) for 20 min at 28°C. The reaction was quenched with 125 mM glycine (in 1× PBS, pH 7.4) for 5 min at room temperature. Cells were harvested by centrifugation at 8,600 g (4°C) for 10 min and washed with 500 ml 20 mM sodium phosphate buffer (pH 7.4) containing 50 mM NaCl and 1 mM EDTA. Cell pellets were resuspended in BugBuster Protein Extraction Reagent (Novagen, Germany) supplemented with 0.5% n-dodecyl-β-maltoside (Thermo Scientific, USA), 100 μg/ml PMSF and Lysonase Bioprocessing Reagent (Merck, Germany). Complete cell lysis was achieved after two passages

through a French press at 16,000 psi, and cell debris was removed by centrifugation at 16,000 g for 20 min at 4°C. One milliliter of precleared cell lysate was then incubated for 60 min at room temperature with Dynabeads crosslinked to a monoclonal anti-His antibody (SIGMA-Aldrich, Germany). Immobilization of the antibody was carried out as described by the manufacturer. The beads were washed three times with 50 mM Tris-HCl (pH 7.5) containing 150 mM NaCl, 1 mM EDTA, 100 μg/ml PMSF and 0.5% n-dodecyl-β-maltoside, and then with 100 mM Tris-HCl (pH 7.5) containing 750 mM NaCl, 1 mM EDTA and 0.05% n-dodecyl-β-maltoside. Precipitated proteins were eluted from the beads with 400 μl of 0.2% formic acid (pH 2.5) and submitted to mass spectrometric analysis.

Fluorescence Microscopy

For light microscopic analyses, cells were spotted onto pads made of 1% agarose (for still images) or 1% agarose in M2G medium (for time-lapse analyses). When appropriate, the cover slides were sealed with VLAP (vaseline, lanolin and paraffin at a 1:1:1 ratio). Images were recorded with either a Zeiss Axio Imager.M1 microscope equipped with a Plan Apochromat 100×/1.40 Oil DIC objective and a Cascade:1K CCD camera (Photometrics), a Zeiss Axio Imager.Z1 microscope equipped with a 100×/1.46 Oil DIC objective and a pco.edge sCMOS camera (PCO), or a Nikon 90i microscope equipped with a 100×/1.40 Oil phase contrast objective and a Rolera XR CCD camera (QImaging). Images were processed with Metamorph 7.1.2 (Universal Imaging Group) or NIS Elements software (Nikon). Photobleaching experiments were performed with either a 561 nm solid state laser and a 2D-VisiFRAP Galvo System multi-point FRAP module (Visitron Systems, Germany), applying strain-dependent pulses at a laser power of 5%, or a MicroPoint laser system (Photonic Instruments, St. Charles, IL) equipped with an NL100 nitrogen laser (Stanford Research Systems, Sunnyvale, CA) and a 551 nm laser dye. Photobleaching experiments with StpX-GFP were performed with a Leica TCS SP5 scanning confocal microscope equipped with a HCX PL APO Lambda Blue 63×/1.40 Oil objective, a 100 mW argon laser and a 10 mW DPSS laser (Leica Microsystems, Bannockburn, IL). Quantification of photobleaching was performed with ImageJ (NIH) and Matlab (Mathworks).

Transmission Electron Microscopy

Transmission electron micrographs of negatively contrasted *Caulobacter* cells were taken with either a Zeiss CEM902 electron microscope, operated at 80 kV and equipped with a wide-angle dual-speed 2K x 2K CCD camera or a JEOL 2100 electron microscope, operated at 80 kV and equipped with a fast-scan 2K x 2K CCD camera F214. Cells were spotted onto carbon-coated grids (100 mesh) and stained with a 1:2 diluted supernatant of saturated uranyl acetate (in dH20). Image processing and the determination of stalk lengths was carried out with Adobe Photoshop CS2 (Adobe Systems) and the MetaMorph 7.1.2 (Universal Imaging Group) region measurement tool. Statistical significance was assessed with a paired t test with Origin 6.1 (OriginLab).

Electron Cryotomography

Electron cryo-tomography (ECT) was performed as described (Möll et al., 2010). Correlated fluorescence light microscopy (FLM) combined with ECT was essentially carried out as reported previously (Ingerson-Mahar et al., 2010), with the exception that cells were immobilized on C flat 2/2 London finder copper TEM grids with a ~40 nm thick holey carbon coat (Protochips Inc., Raleigh, NC, USA), which were treated with 5 μl of 1 mg/ml sterile-filtered poly-L-lysine (Sigma P1524) before use. The correlative analysis was performed manually with the Adobe Photoshop software (Adobe Systems). The prominent holes in the carbon foil together with the cell body and stalk densities were sufficient to unambiguously overlay the FLM images and the ECT slices. Three-dimensional reconstructions were calculated with IMOD (Mastronarde, 2005), RAPTOR (Amat et al., 2008) or Tomo3D (Agulleiro and Fernandez, 2011). Segmentation and 3D visualization were carried out manually with Amira (Mercury Computer Systems).

SUPPLEMENTAL REFERENCES

Agulleiro, J.I., and Fernandez, J.J. (2011). Fast tomographic reconstruction on multicore computers. Bioinformatics *27*, 582–583.

Amat, F., Moussavi, F., Comolli, L.R., Elidan, G., Downing, K.H., and Horowitz, M. (2008). Markov random field based automatic image alignment for electron tomography. J. Struct. Biol. *161*, 260–275.

Botstein, K., Lew, K.K., Jarvik, V., and Swanson, C.A. (1975). Role of antirepressor in the bipartite control of repression and immunity by bacteriophage P22. J. Mol. Biol. *91*, 439–462.

Chen, J.C., Viollier, P.H., and Shapiro, L. (2005). A membrane metalloprotease participates in the sequential degradation of a *Caulobacter* polarity determinant. Mol. Microbiol. *55*, 1085–1103.

Domian, I.J., Quon, K.C., and Shapiro, L. (1997). Cell type-specific phosphorylation and proteolysis of a transcriptional regulator controls the G1-to-S transition in a bacterial cell cycle. Cell *90*, 415–424.

Ely, B. (1991). Genetics of *Caulobacter crescentus*. Methods Enzymol. *204*, 372–384.

Hughes, H.V., Huitema, E., Pritchard, S., Keiler, K.C., Brun, Y.V., and Viollier, P.H. (2010). Protein localization and dynamics within a bacterial organelle. Proc. Natl. Acad. Sci. USA *107*, 5599–5604.

Ingerson-Mahar, M., Briegel, A., Werner, J.N., Jensen, G.J., and Gitai, Z. (2010). The metabolic enzyme CTP synthase forms cytoskeletal filaments. Nat. Cell Biol. *12*, 739–746.

Kühn, J., Briegel, A., Mörschel, E., Kahnt, J., Leser, K., Wick, S., Jensen, G.J., and Thanbichler, M. (2010). Bactofilins, a ubiquitous class of cytoskeletal proteins mediating polar localization of a cell wall synthase in *Caulobacter crescentus*. EMBO J. *29*, 327–339.

Mastronarde, D.N. (2005). Automated electron microscope tomography using robust prediction of specimen movements. J. Struct. Biol. *152*, 36–51.

Meisenzahl, A.C., Shapiro, L., and Jenal, U. (1997). Isolation and characterization of a xylose-dependent promoter from *Caulobacter crescentus*. J. Bacteriol. *179*, 592–600.

Möll, A., Schlimpert, S., Briegel, A., Jensen, G.J., and Thanbichler, M. (2010). DipM, a new factor required for peptidoglycan remodelling during cell division in *Caulobacter crescentus*. Mol. Microbiol. *77*, 90–107.

Poindexter, J.S. (1964). Biological Properties and Classification of the *Caulobacter* Group. Bacteriol. Rev. *28*, 231–295.

Poindexter, J.S. (1978). Selection for nonbuoyant morphological mutants of *Caulobacter crescentus*. J. Bacteriol. *135*, 1141–1145.

Radhakrishnan, S.K., Thanbichler, M., and Viollier, P.H. (2008). The dynamic interplay between a cell fate determinant and a lysozyme homolog drives the asymmetric division cycle of *Caulobacter crescentus*. Genes Dev. *22*, 212–225.

Thanbichler, M., and Shapiro, L. (2006). MipZ, a spatial regulator coordinating chromosome segregation with cell division in *Caulobacter*. Cell *126*, 147–162.

Tsai, J.W., and Alley, M.R. (2001). Proteolysis of the Caulobacter McpA chemoreceptor is cell cycle regulated by a ClpX-dependent pathway. J. Bacteriol. *183*, 5001–5007.

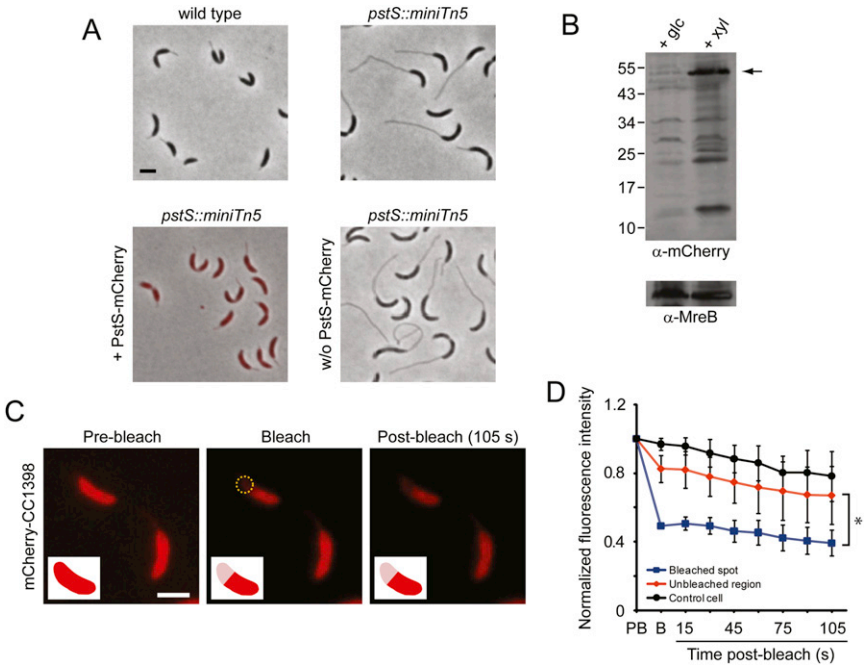

Figure S1. PstS-mCherry Is Functional and FRAP Methodology Can Bleach a Subcellular Region, Related to Figure 1

(A) Functionality of the PstS-mCherry fusion. The indicated strains were grown overnight in PYE and images were captured to assess stalk length. Loss of *pstS* (EK425) leads to stalk elongation as a result of defective phosphate uptake. Xylose-mediated induction of PstS-mCherry (EK424) complements the *pstS* mutant phenotype and reverts the stalks to normal length. Scale bar, 2 μm.

(B) Western blot analysis of strain EK424 showing that the majority of PstS-mCherry is full length (arrow) when cells are grown with 0.3% xylose. The same sample was analyzed with an anti-MreB antibody as a loading control.

(C) FRAP analysis on fixed cells. Cells expressing mCherry-CC1398 (EK61) were fixed in 3.7% formaldehyde to inhibit protein diffusion and analyzed by FRAP. Cells were bleached once where indicated by a dashed circle, followed by a 105 s recovery period. Insets show schematic representations of the results. Note, CC1398 is a so far uncharacterized freely diffusible protein.

(D) Quantification of fluorescence intensities from multiple FRAP experiments (n = 4; *$p < 0.02$; error bars = SD). Cells expressing mCherry-CC1398 were treated as described in (C), and fluorescence intensities were measured in the bleached (blue) and unbleached region (red) of the bleached cell or in the cell body of a nearby control cell (black). To compare the recovery of fluorescence in several cells, the fluorescence intensity of each region of interest was normalized to its pre-bleach intensity. Scale bars, 2 μm.

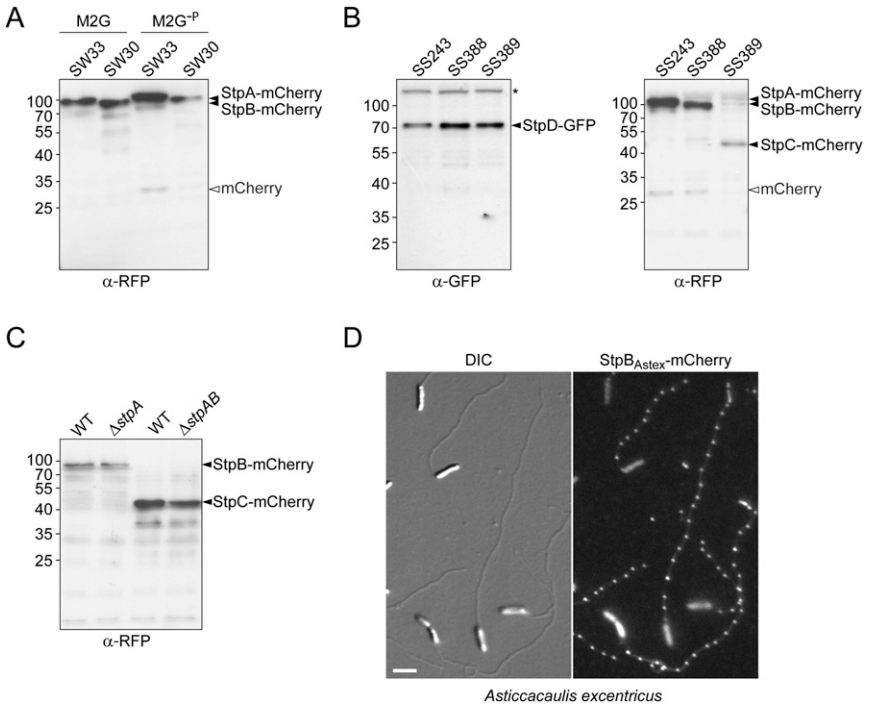

Figure S2. Stability and Cross-Band-like Subcellular Localization of Stp Proteins, Related to Figure 2

(A) Western blot analysis of strain SW33 (P_{xyl}::P_{xyl}-*stpA-mcherry*) and SW30 (P_{xyl}::P_{xyl}-*stpB-mcherry*) cultured for 24h in high-phosphate (M2G) and low-phosphate ($M2G^{-P}$) medium containing 0.3% xylose to induce production of the fluorescent protein fusions. Filled arrowheads indicate full-length StpA-mCherry or StpB-mCherry. Empty arrowheads point to clipped mCherry.

(B) Western blot analysis of strain SS243 (*stpD;;stpD-gfp* P_{xyl}::P_{xyl}-*stpA-mcherry*), SS388 (*stpB;;stpB-mcherry stpD;;stpD-gfp*) and SS389 (*stpC::stpC-mcherry stpD;;stpD-gfp*) showing the stable production of StpD-GFP (left panel) and StpA-mCherry, StpB-mCherry and StpC-mCherry (right panel). Cells were grown in $M2G^{-P}$ for 24h. Synthesis of StpA-mCherrry was induced by adding 0.3% xylose for 24 hr. Samples were analyzed with an anti-GFP and anti-RFP antibody, respectively. Filled arrowheads indicate the full-length fusion proteins. The empty arrowhead points to clipped mCherry. The asterisk denotes a non-specific signal.

(C) Western blot analysis of strains SS412 to SS415 showing the levels of StpB-mCherry and StpC-mCherry when produced from their endogenous promoters in a wild-type or a Δ*stpA* or Δ*stpAB* mutant background. Cells were grown to exponential phase in PYE medium. Samples were probed with an anti-RFP antibody. Filled arrowheads indicate the full-length fusion proteins.

(D) Cells of *Asticcacaulis excentricus* CB48 carrying a mCherry-tagged version of the StpB homolog Astex_0987 (SS309) were cultured in $M2G^{-P}$ and imaged by DIC and fluorescence microscopy. Scale bar, 3 μm.

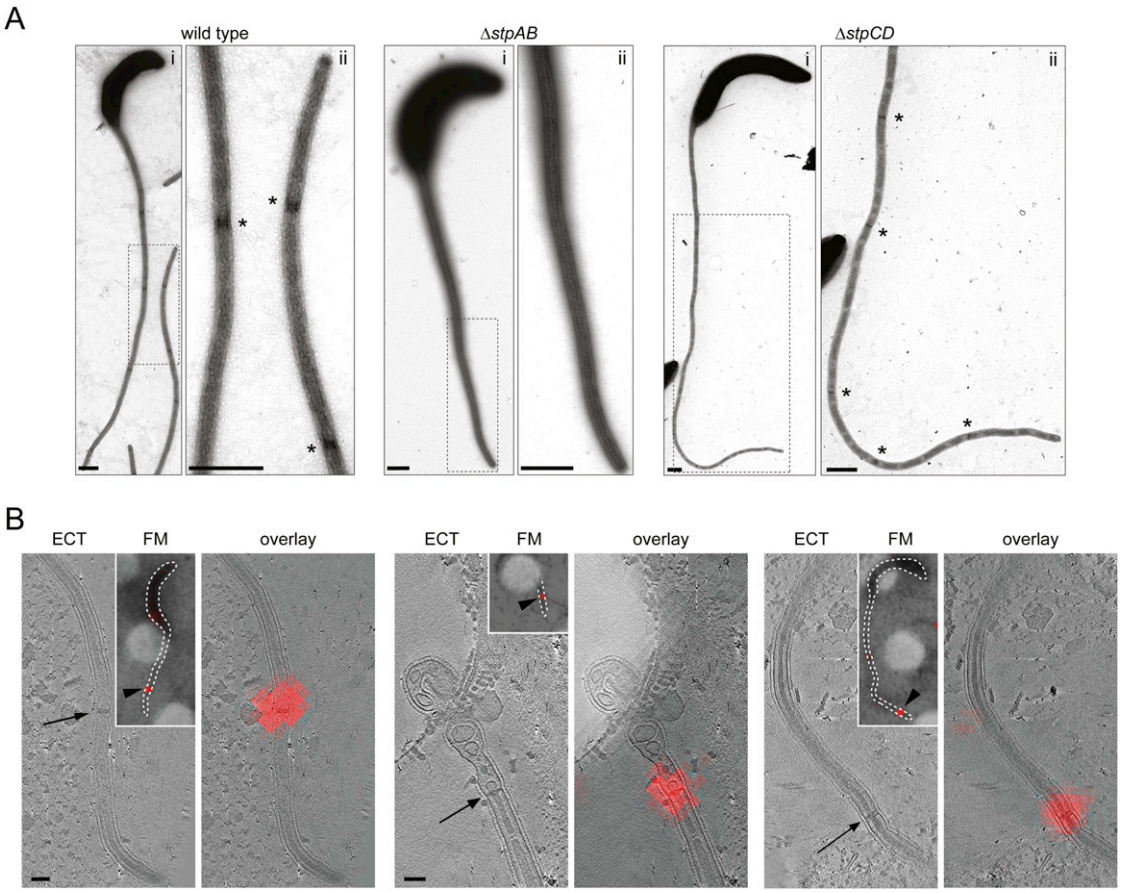

Figure S3. Stp Proteins Are Required for Cross-Band Formation and Colocalize with Cross-Bands, Related to Figure 3

(A) Representative electron micrographs of negatively stained wild-type, Δ*stpAB* (SW51, n = 58) and Δ*stpCD* (SS250, n = 42) cells grown in $M2G^{-P}$ medium. The dashed rectangle in (i) indicates the region magnified in (ii). Asterisks denote cross-bands. Scale bars, 500 nm.

(B) Representative images showing the colocalization of StpB-mCherry with cross-bands (arrows). Cells (SW30) were grown in $M2G^{-P}$ medium with 0.3% xylose and analyzed by correlated fluorescence microscopy (FM) and electron cryo-tomography (ECT). Insets show overlays of phase contrast and fluorescence images, with arrowheads indicating the cross-band visualized in the correlated ECT/FM images (arrows). Scale bars, 100 nm.

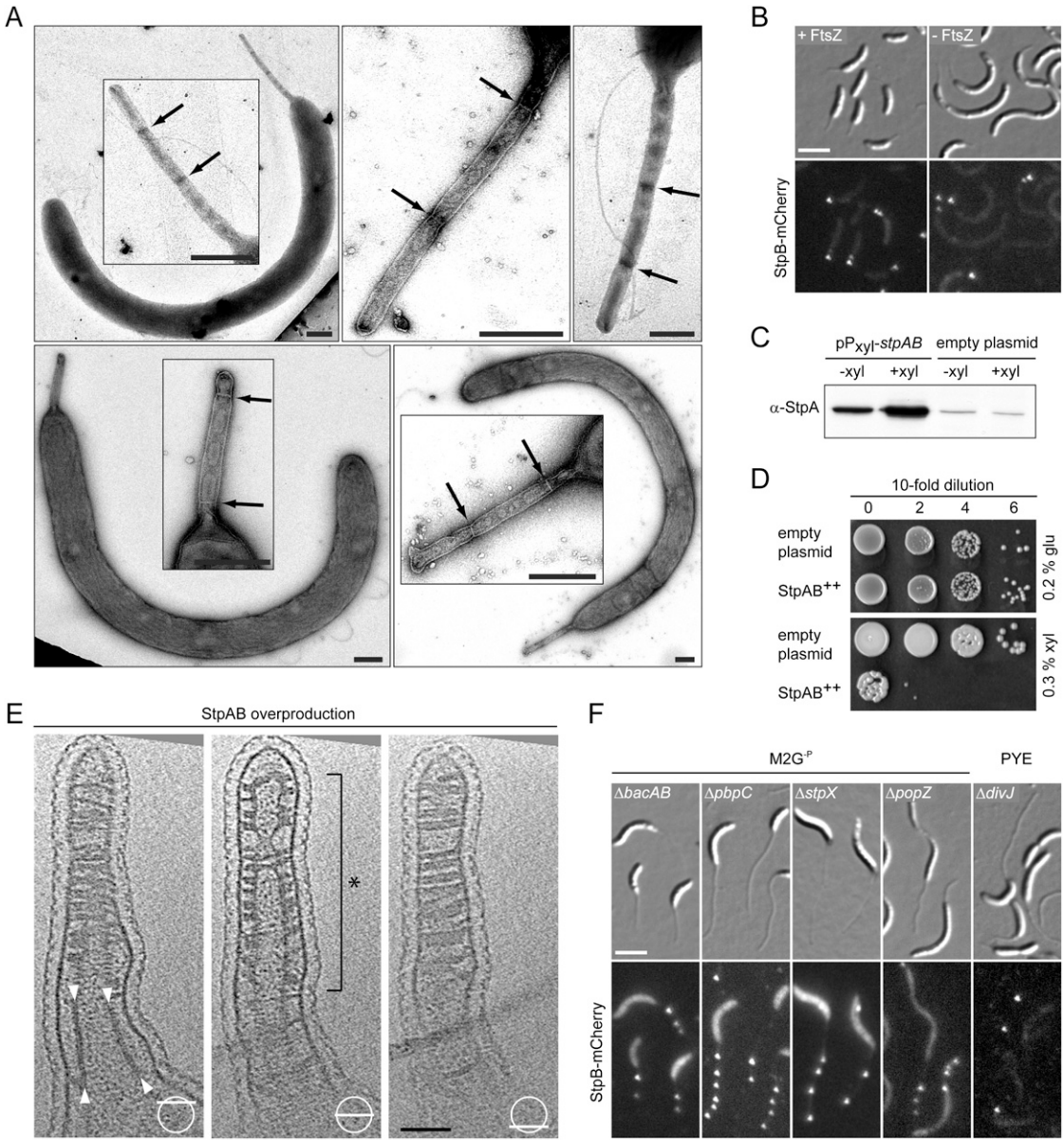

Figure S4. Cross-Band Formation Is Independent of FtsZ and Polar Localizing Proteins, Related to Figure 4

(A) Presence of cross-bands in cells depleted of FtsZ. Swarmer cells of strain SS191 (*ftsZ*::Pxyl-*ftsZ* P_{van}::P_{van}-*stpB-mcherry*) were released into inducer-free M2G medium to suppress FtsZ synthesis, incubated for 6 hr, negatively stained with uranylacetate, and visualized by electron microscopy. Insets show magnifications of the stalks. Arrows point to cross-bands. Scale bars, 500 nm. Note that swarmer cells are largely devoid of FtsZ.

(B) Formation of Stp complexes in the absence of FtsZ. Isolated swarmer cells of strain SS191 (*ftsZ*::Pxyl-*ftsZ* P_{van}::P_{van}-*stpB-mcherry*) were released into M2G medium with and without 0.3% xylose. After 6 hr of incubation, cells were imaged by DIC and fluorescence microscopy. StpB-mCherry production was induced with 0.5 mM vanillate for 2h prior to imaging. Scale bars, 3 μm.

(C) Western blot analysis of cells carrying the *stpAB* overexpression plasmid pP_{xyl}-*stpAB* (SS214) or the corresponding empty plasmid (SS258) showing StpA levels during growth in the absence or presence of 0.3% xylose.

(D) Spot assay showing the viability of strains SS214 (pP_{xyl}-*stpAB*) and SS258 (empty plasmid) upon overproduction of StpAB. Cells were grown in PYE for 24 hr, diluted to an OD600 of 0.16, subjected to the indicated number of serial 10-fold dilutions, and spotted on PYE agar containing either 0.2% glucose or 0.3% xylose.

(E) Representative tomographic slices (top, middle and bottom) through the stalk of a StpAB-overproducing cell. Cells carrying a plasmid-encoded copy of *stpAB* under the control of P_{xyl} (SS214) were pre-cultured in PYE medium and then grown in $M2G^{-P}$ medium containing 0.3% xylose. White arrowheads point to additional densities lining the cytoplasmic membrane. The section used for 3D-reconstruction and image segmentation in Figure 4F and Movie S5 is indicated by an asterisk. Scale bar, 50 nm.

(F) StpB-mCherry shows the normal stalk localization pattern in the absence of BacAB (SS281), PbpC (SS167), StpX (SS213), PopZ (SS292) or DivJ (SS224). Cells were grown for 24 hr in $M2G^{-P}$ medium with 0.3% xylose or to exponential phase in PYE medium with 0.3% xylose. Scale bar, 3 μm.

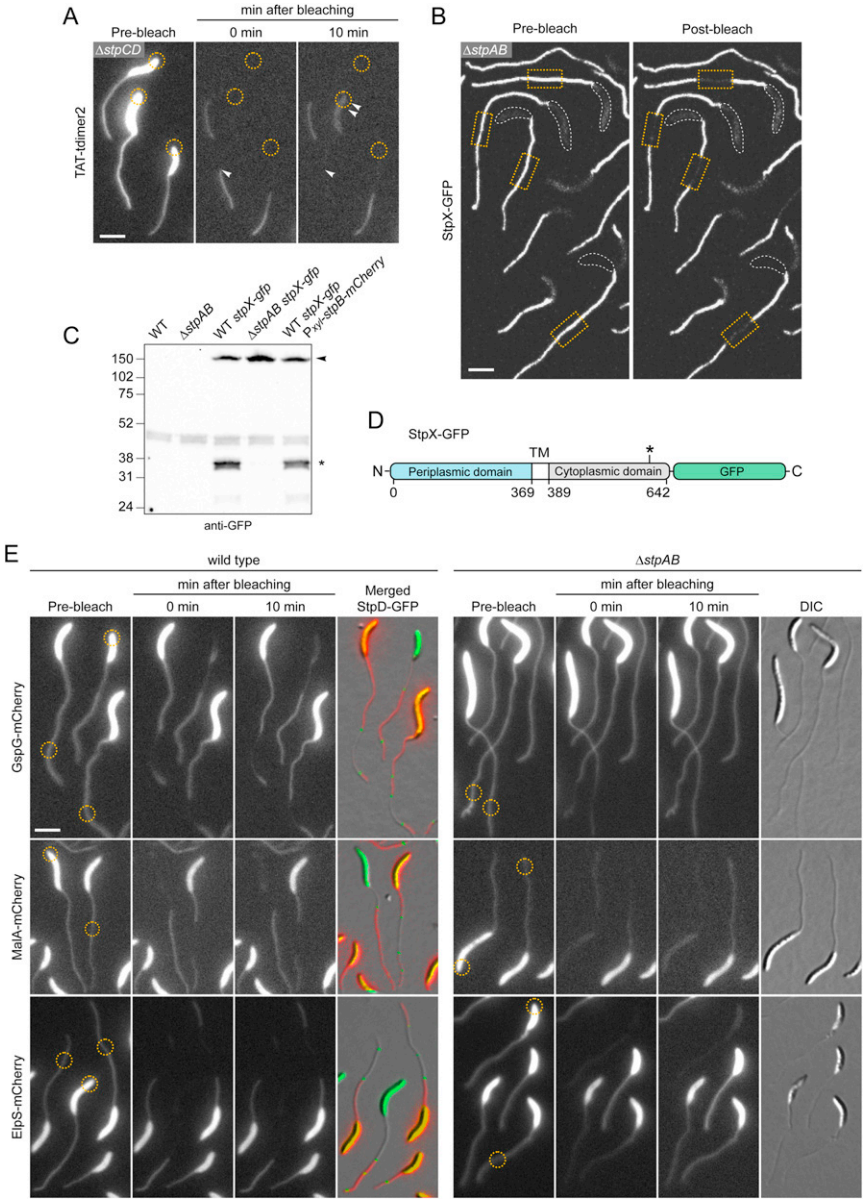

Figure S5. Cross-Bands Act as Protein Diffusion Barriers, Related to Figure 5

(A) The mobility of TAT-tdimer2 was impaired in about 50% of the cells lacking StpC and StpD (SS304). After cells had been grown in $M2G^{-P}$ medium with 0.3% xylose for 24-30 hr and mounted on an agarose pad, the diffusion of TAT-tdimer2 was assessed by FLIP analysis (n = 122 cells). A laser pulse was applied to the regions indicated by a yellow circle. Cells were visualized by DIC and fluorescence microscopy before and after photobleaching. White arrowheads point to a representative cell with a leaky diffusion barrier. Scale bar, 3 μm.

(B) StpX is immobile in StpAB-deficient cells. Cells of a Δ*stpAB* strain expressing StpX-GFP under the control of the native *stpX* promoter (YB5059) were grown in HIGG medium containing 30 μM phosphate, mounted on agarose pads, and subjected to FLIP analysis. Orange rectangles indicate regions that were bleached for 52 s, followed by acquisition of a post-bleach image. Scale bar, 3 μm.

(C) Processing of StpX-GFP is abolished in the absence of cross-bands. Whole-cell lysates of the indicated strains were probed with an anti-GFP antibody (JL-8 monoclonal, Clontech), which detects the cytoplasmic C terminus of the StpX-GFP fusion. The arrowhead indicates the full-length fusion, the asterisk the dominant short fragment.

(D) Schematic of the StpX-GFP fusion used in this study. The asterisk indicates the approximate position of the cleavage site that results in the ~35 kDa cytoplasmic fragment detected by western blot analysis in (C). Numbers indicate the positions of the amino acid residues at the boundaries of the different domains.

(E) FLIP experiments testing the mobility of inducible fluorescent protein fusions to the inner membrane protein GspG and the two outer membrane proteins ElpS and MalA in the presence (SS277, SS283, SS297) and absence (SS272, SS284, SS294) of the Stp complex. Cells were treated as in (A). Yellow circles denote bleached regions. In the overlays shown for wild-type cells producing GspG-mCherry, MalA-mCherry or ElpS-mCherry (red), cross-bands were visualized with a StpD-GFP fusion (green). Scale bar, 3 μm.

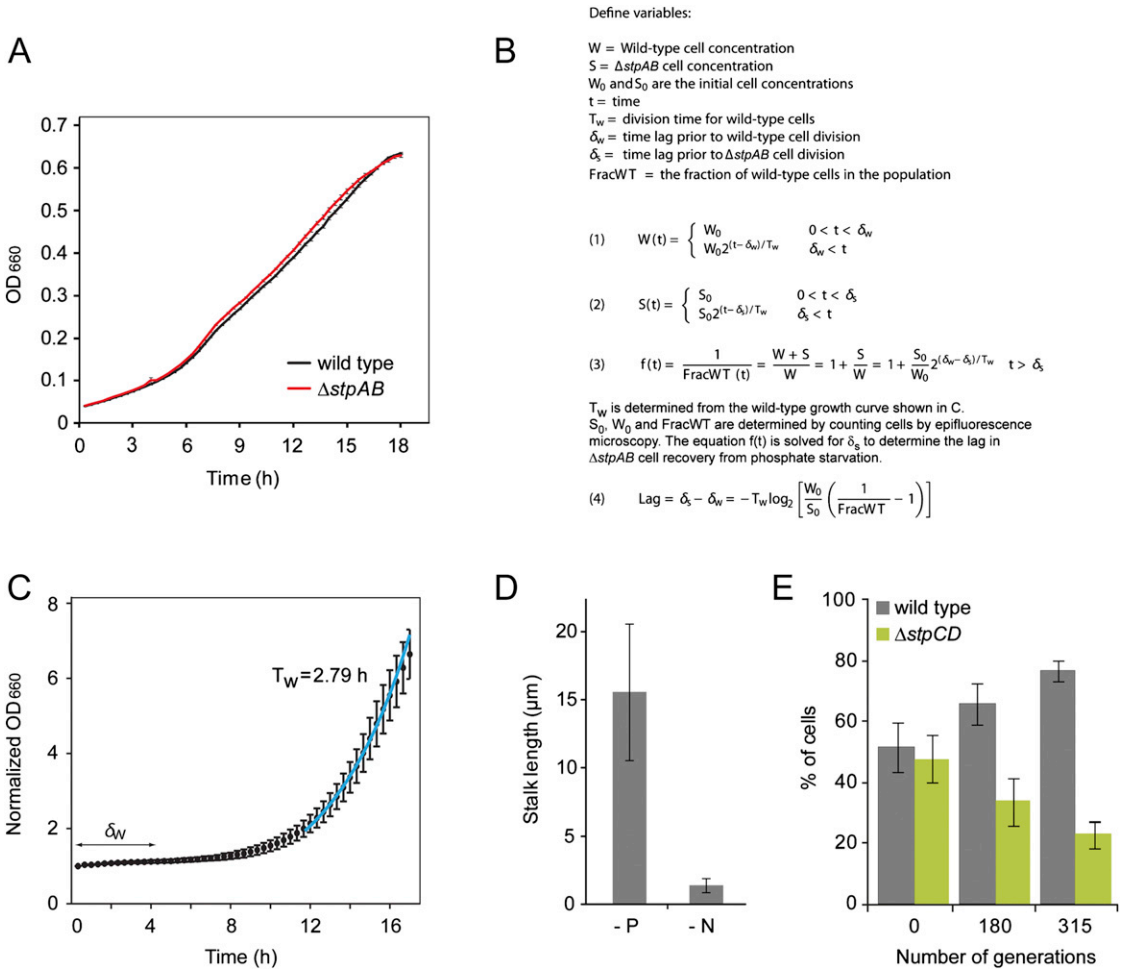

Figure S6. Wild-Type Cells Outcompete Diffusion Barrier-Deficient Mutants, Related to Figure 6

(A) Wild-type and Δ*stpAB* (SW51) cells have equal growth rates. Cells were grown in HIGG-200 μM phosphate (n = 10 for each strain, error bars = SEM). Optical density was monitored over 18 hr in a microplate shaker/reader (Biotek). Note, Δ*stpCD* (SS250) cells show similar growth rates in high-phosphate medium (data not shown).

(B) Equations developed to determine the relative growth lag between wild-type and StpAB-deficient cells after transfer from low-phosphate to phosphate-rich medium. The lag between wild-type and StpCD-deficient cells was determined in an analogous manner.

(C) Determination of the parameters required to solve the equations shown in (B). The doubling time of the wild-type strain was estimated by growing cells overnight in HIGG-30 nM phosphate followed by dilution to an OD_{660} of 0.1 in HIGG-200 μM phosphate. Optical density was monitored over 18 hr in a microplate shaker/reader. The exponential growth rate was determined by fitting the curve to the equation $y = a*2^{t/Tw}$. The fitted line corresponds to a doubling time (Tw) of 2.79 hr.

(D) Stalk lengths measured for wild-type cells (CB15N) after 4 days of phosphate (- P) or nitrogen (- N) starvation (n = 35; error bars = SD).

(E) Wild-type cells outcompete a mutant with leaky diffusion barriers. Wild-type and Δ*stpCD* (SS250) cells were grown in PYE medium and mixed at equal optical densities. The mixed cultures (n = 3) were repeatedly diluted into fresh PYE medium and cultured to stationary phase. At the indicated time points, cells were withdrawn and spread on PYE agar. The ratio of wild-type to barrier-defective cells was determined by colony PCR (n ~360; error bars = SD).